AD-A048 779 GENERAL ELECTRIC CO PHILADELPHIA PA SPACE DIV F/G 20/5
CHEMICAL LASER POTENTIAL OF SELECTED GROUP IV-A METAL OXIDES.(U)
NOV 77 M J LINEVSKY, R A CARABETTA F29601-76-C-0055
UNCLASSIFIED AFWL-TR-77-121 NL

1 OF 1
AD
A048779

END
DATE
FILMED
2-78
DDC

AFWL-TR-77-121

AFWL-TR-
77-121

DDC

(2)

SC

CHEMICAL LASER POTENTIAL OF SELECTED GROUP IV-A METAL OXIDES

November 1977

Final Report

Approved for public release; distribution unlimited.

AIR FORCE WEAPONS LABORATORY
Air Force Systems Command
Kirtland Air Force Base, NM 87117

This final report was prepared by the General Electric Company, Valley Forge Space Center, Philadelphia, Pennsylvania, under Contract F29601-76-C-0055, Job Order 12560308 with the Air Force Laboratory, Kirtland Air Force Base, New Mexico. Major Bousek (ALC) is the Laboratory Project Officer-in-Charge.

When US Government drawings, specifications, or other data are used for any purpose other than a definitely related Government procurement operation, the Government thereby incurs no responsibility nor any obligation whatsoever, and the fact that the Government may have formulated, furnished, or in any way supplied the said drawings, specifications, or other data is not to be regarded by implication or otherwise as in any manner licensing the holder or any other person or corporation or conveying any rights or permission to manufacture, use, or sell any patented invention that may in any way be related thereto.

This report has been reviewed by the Office of Information (OI) and is releasable to the National Technical Information Service (NTIS). At NTIS, it will be available to the general public, including foreign nations.

This technical report has been reviewed and is approved for publication.

Ronald R. Bousek

RONALD R. BOUSEK,
Major, USAF
Project Officer

FOR THE COMMANDER

Armand D. Maio

CARL A. FORBRICH,
Major, USAF
Chief, Chemical Laser Branch

ARMAND D. MAIO,
Lt Col, USAF,
Chief, Advanced Laser Technology Division

DO NOT RETURN THIS COPY. RETAIN OR DESTROY

(18) AFWL, SBIE

UNCLASSIFIED

SECURITY CLASSIFICATION OF THIS PAGE (When Data Entered)

(19) REPORT DOCUMENTATION PAGE

READ INSTRUCTIONS BEFORE COMPLETING FORM

1. REPORT NUMBER: AFWL-TR-77-121, AD-E200 076

2. GOVT ACCESSION NO.

3. RECIPIENT'S CATALOG NUMBER

4. TITLE (and Subtitle): (6) CHEMICAL LASER POTENTIAL OF SELECTED GROUP IV-A METAL OXIDES.

5. TYPE OF REPORT & PERIOD COVERED: (9) Final Report

6. PERFORMING ORG. REPORT NUMBER

7. AUTHOR(s): (10) M.J. Linevsky [redacted] R.A. Carabetta

8. CONTRACT OR GRANT NUMBER(s): (15) F29601-76-C-0055

9. PERFORMING ORGANIZATION NAME AND ADDRESS
General Electric Company
Space Division, Space Sciences Laboratory
P.O. Box 8555, Philadelphia, Pa. 19101

10. PROGRAM ELEMENT, PROJECT, TASK AREA & WORK UNIT NUMBERS
Program Element: 62301E
JON: 1256[redacted] (16) (17) 03

11. CONTROLLING OFFICE NAME AND ADDRESS
Air Force Weapons Laboratory
Kirtland Air Force Base, NM 87117

12. REPORT DATE: (11) Nov 77

13. NUMBER OF PAGES: (12) 69p.

14. MONITORING AGENCY NAME & ADDRESS (if different from Controlling Office)
Air Force Weapons Laboratory
Kirtland Air Force Base, NM 87117

15. SECURITY CLASS. (of this report): Unclassified

15a. DECLASSIFICATION/DOWNGRADING SCHEDULE

16. DISTRIBUTION STATEMENT (of this Report)
Approved for public release; distribution unlimited.

17. DISTRIBUTION STATEMENT (of the abstract entered in Block 20, if different from Report)

18. SUPPLEMENTARY NOTES

19. KEY WORDS (Continue on reverse side if necessary and identify by block number)
Chemical Laser
Photon Yields
H_2/N_2O Flames,
SnO
Spectra
GeO
Kinetics
Chemiluminescence

20. ABSTRACT (Continue on reverse side if necessary and identify by block number)

The results of a study investigating the potential of several Group IV-A metal oxides, including SnO* and GeO*, for producing an electronic transition visible chemical laser are discussed in this report. The Sn/SnO* system was studied in H_2/N_2O/He flames containing $SnCl_4$ or $Sn(CH_3)_4$, and in a fast flow reactor in which tin atoms were generated directly and mixed with N_2O. The results of the flame experiments showed that $SnO(a^3\Sigma)$ was rapidly quenched by H_2, that the maximum concentrations of Sn in the gases were limited to ca

DD FORM 1 JAN 73 1473 EDITION OF 1 NOV 65 IS OBSOLETE

UNCLASSIFIED

SECURITY CLASSIFICATION OF THIS PAGE (When Data Entered)

405025

10^{13}/cc, and that laser conditions could not be achieved in the flames. The flow reactor experiments confirmed H_2 quenching of SnO*, and provided evidence that reaction between $Sn(^3P_1)$ and SnO $(a^3\Sigma)$ were measured.

The flame studies on GeO* and SiO* indicated that the Ge/N_2O and Si/N_2O reactions are not promising pumping sources for chemical visible lasers.

Suggestions are made for an SnO* gain experiment.

SUMMARY

The objective of this program was to obtain experimental data on selected Group IV-A metal/N_2O reaction systems which would permit an evaluation of their potential as laser pumping reactions. Premixed low-pressure H_2/N_2O flames containing metal additives have been studied as sources for producing high column densities of electronically excited GeO, SiO, and SnO, and as a means for investigating the behavior of the Sn/SnO($a^3\Sigma$) interactions at relatively high concentrations of SnO_x. In addition to the flame work, which constituted the major part of this program, a relatively modest effort to study the individual rates of reaction of Sn($^3P_0$) and ($^3P_1$) with N_2O, and the quenching of Sn($^3P_1$) and SnO($a^3\Sigma$) by a number of species was also carried out utilizing a flow reactor.

The $SnCl_4$ and $Sn(CH_3)_4$ were added to H_2/N_2O flames diluted with helium and burned at pressures of from 9-15 torr. It was found that the additives were reduced to free metal atoms in the preheat zone of the flames and that the resulting atoms reacted with the unburned N_2O to produce electronically excited SnO. In all flames, and for both additives, strong chemiluminescent emission was observed from the SnO(a→X), (b→X), (b'→X) and (A→X) electronic transitions.

Spatially resolved measurements have been made of the tin atom concentrations, the tin electronic temperature, the absolute SnO(a→X) emission, the flame kinetic temperature and, in some cases, the ground state SnO(X) concentrations. Tin atoms and SnO(X) concentrations were obtained from absorption measurements using experimentally determined curves of growth. These measurements were made at several positions (times) along the flame profile and for a number of total tin (additive) concentrations.

It was found that the maximum concentrations of Sn atoms that could be produced in the flames, ca 10^{13}/cc, was limited by either (tin) particulate formation or by reactions involving Sn and SnO_x species. The photon yield measurements showed that although the initial formation of SnO($a^3\Sigma$) was characterized by high, ca 50%, branching ratio the concentrations of this species in the downstream flame gases were quenched collisionally or reactively by a process involving H_2 with k_Q, $H_2 \sim 5 \times 10^{-11} \exp(-3400/T)$ cc/molec second. Experiments at high total SnO_x concentrations indicated that SnO($a^3\Sigma$) is not measurably quenched by other tin species present in the flame. Quenching by H_2O and O_2 was briefly investigated; it

was found that although O_2 reacts with Sn, neither of these species appreciably quenches $SnO(a^3\Sigma)$.

Gain/loss measurements on the $SnO(a^3\Sigma)$ transitions were carried out by placing the flame gases inside the cavity of a dye laser. Neither gain nor loss could be recorded. It was concluded that the flame was incapable of producing the $SnO(a^3\Sigma)$ concentrations required for lasing.

The experiments on the germanium system paralleled those which were made for SnO. The addition of either GeH_4 or $GeCl_4$ resulted in GeO(a→X), (b→X) and (A→X) chemiluminescence in the preheat zone of the H_2/N_2O/He flames. As for $SnO(a^3\Sigma)$, it was found that $GeO(a^3\Sigma)$ is rapidly quenched by H_2 in the flame gases and that the rate constant for this process is about 1.1×10^{-12} exp(-837/T) cc/molec second. Measurement of the system photon yields and of the photon yield of $GeO(a^3\Sigma)$ at the plane of maximum emission in the flames were disappointingly low, about 0.03%. On this basis it was concluded that the production of $GeO(a^3\Sigma)$ by the reaction of Ge with N_2O is not a promising pumping source.

Emission from the SiO(a→X) transitions was not observed when either $SiCl_4$ or SiH_4 were added to the flames and detailed experiments on this system were not carried out.

The direct reactions of $Sn(^3P_1)$ and $(^3P_0)$ with N_2O were studied in the flow reactor at pressures of from about 3 to 11 torr, for linear velocities of from 50 to 150 meters/second, and at temperatures of 300 and 500 °K. Examination of the chemiluminescent emission showed that the only excited state produced under these conditions was $SnO(a^3\Sigma)$. Measurements of the $Sn(^3P_0)$ and $(^3P_1)$ concentrations showed that their nonequilibrium population distribution in the flow were functions of the gas composition, flow velocity, and the temperature of the Sn atom source. It was possible to measure the rate constants for the quenching of $^3P_1$ by H_2, N_2, and N_2O at a temperature of 550 °K; the resulting values are (in units cc/molec second): $k_Q^{H_2} = 5.0 \pm 1.2 \times 10^{-12}$; $k_Q^{N_2} = 0.9 \pm 0.2 \times 10^{-12}$ and $k_Q^{N_2O} = 1.3 \times 10^{-12}$. From measurements of the Sn populations and the absolute $SnO(a^3\Sigma)$ emission intensity it was possible to show that the rate constant for the reaction of $Sn(^3P_1)$ with N_2O to form $SnO(a^3\Sigma)$ is 2.8×10^{-11} exp(-1990/T) cc/molec second, and that the branching ratio at 550 °K is 0.7 ± 0.4. The rate constant for the reaction $Sn(^3P_0)$ with N_2O was estimated to be about a factor of 25 less than that of the $^3P_1/N_2O$ re-

action and that for the quenching of $SnO(a^3\Sigma)$ by H_2 was found to be about 3.4 ± 10^{-13} cc/molec second at 550°K.

The flame experiments were reinterpreted using the $Sn(^3P_1)/N_2O$ rate constants obtained with the flow reactor. It was found that the quenching of SnO by H_2 was more severe than that derived from the original treatment of the flame data.

It is concluded that the flame approach offers little hope for the production of a metal oxide electronic transition chemical laser. However, the direct reaction of $Sn(^3P_1)$ with N_2O in a fast flow configuration offers a high probability for achieving gain in the $a^3\Sigma$ state of SnO. A proof-of-principle experiment is suggested.

CONTENTS

ILLUSTRATIONS

TABLES

SECTION I

INTRODUCTION

At the start of this program, evidence existed (ref. 1) that the gas phase reactions of certain Group IV-A metals with N_2O led to the production of electronically excited metal oxide species which appeared attractive as active molecules for electronic transition chemical lasers. Of the three metals for which excited metal oxide production had been observed; namely Si, Ge and Sn, the reaction of Sn with N_2O seemed especially promising as a laser pumping reaction. Specifically, it was found that the principal product of the Sn/N_2O reaction is the moderately long-lived $a^3\Sigma$ state of SnO, and that this species is relatively immune to quenching by N_2O and N_2 which are also present in the gas flow. Although the reactions of Ge and Si with N_2O were also known to produce $GeO(a^3\Sigma)$ and $SiO(a^3\Sigma)$, the kinetics of these processes had not ben quantitatively studied.

With regard to their potential as laser species, the Group IV-A oxides possess some very attractive properties. The metastability of their lowest lying excited ($^3\Sigma$) states is favorable from a practical point of view because it relaxes somewhat the metal/N_2O mixing requirements in a working cw laser; i.e., the loss of excited species by radiative decay during this period of formation can be quite small. In addition, the equilibrium internuclear separation of the $^3\Sigma$ and of the $^1\Sigma$ (ground) states are favorably displaced relative to each other. As a result, the largest Franck-Condon factors for the $SnO(a\rightarrow X)$, $GeO(a\rightarrow X)$ and $SiO(a\rightarrow X)$ emissions are those associated with transitions originating from low vibrational levels of the excited state and terminating in high vibrational levels of the ground state — a circumstance which enhances the possibility of achieving substantial gain in these electronic systems.

An inherent difficulty associated with the use of Sn, Ge, and Si as sources of excited species is that of producing the relatively high column densities of free metal which are required to establish gain in the corresponding oxides. In a previous study (ref. 1), several different methods of producing high concentrations of these low vapor pressure metals were attempted. The most promising involved the introduction of volatile compounds of tin, germanium, and silicon into low pressure H_2/N_2O flames. It was found that materials such as $SnCl_4$ and $GeCl_4$ were rapidly

reduced to free metal atoms in the preheat zone and that the resulting atoms subsequently reacted with N_2O to produce electronically excited metal oxides.

This program consists of two parts. In the first part, which represents a continuation of the earlier flame work, attempts were made to produce high column densities of Sn/SnO*, Si/SiO* and Ge/GeO* in H_2/N_2O flames containing metal additives. Quantitative measurements on the kinetic behavior of these species were carried out to determine their lasing potential in this environment. In the second part, detailed measurements on the reactions of $Sn(^3P_0)$ and $(^3P_1)$ with N_2O were carried out using a fast flow reactor and a tin atom generator. Rate constants of processes bearing on the production and quenching of $SnO(^3\Sigma)$ were determined.

SECTION II

FLAME STUDIES

1. BACKGROUND AND INTRODUCTION

In work performed previously (ref. 1), relatively strong metal oxide emissions were observed in low pressure H_2/N_2O flames containing additives such as $SnCl_4$ and $GeCl_4$. Specifically, it was found that the addition of these metal compounds resulted in two distinct zones of luminosity in the flames; the first peaked and decayed entirely within the preheat zone, while the second coincided with the reaction zone of the flames. Based on a number of observations, it was concluded that the mechanism giving rise to the excitation of GeO and SnO in the preheat zone involved the reduction of metal additives by H-atoms to produce free metal atoms, and the subsequent reoxidation of the metal by N_2O to yield chemiluminescent emissions. It was also concluded that the metal oxide emission in the reaction zone arose principally as a result of three body recombination reactions involving metal oxide species and flame free radicals.

Spatially and spectrally resolved measurements on the $SnCl_4/H_2/N_2O$ flames showed that the emissions from the preheat zone consisted primarily of the $(a^3\Sigma \rightarrow X^1\Sigma)$, $(b^3\Pi \rightarrow X^1\Sigma)$, $(b' \rightarrow X^1\Sigma)$ and $(A^1\Pi \rightarrow X^1\Sigma)$* transitions of SnO, and that the emission from the reaction zone contained banded components, namely, the $(b' \rightarrow X^1\Sigma)$ and $(A^1\Pi \rightarrow X^1\Sigma)$ transition of SnO, and a strong underlying continuum possibly polyatomic in origin. Similar measurements on the $GeCl_4/H_2/N_2O$ flames showed that the $(a^3\Sigma \rightarrow X^1\Sigma)$ and $(A^1\Pi \rightarrow X^1\Sigma)$ transitions of GeO comprised the banded structure observed in the preheat zone, and that the reaction zone emission was entirely continuous. Preliminary measurements carried out on the $SiCl_4/H_2/N_2O$ system indicated that it was not possible to reduce $SiCl_4$ to Si by H-atoms and as a result no information on SiO chemiluminescence was obtained.

Following these initial surveys, more detailed measurements were carried out in the $SnCl_4/H_2/N_2O$ flames. Based on a preliminary vibrational assignment of the $SnO(a \rightarrow X)$ transitions, molecular constants were determined for the $SnO(a^3\Sigma)$ state.

---

*Note that these transitions have previously (refs. 1,2) been referred to as $(a \rightarrow X)$, $(B \rightarrow X)$, $(C \rightarrow X)$, and $(D \rightarrow X)$, respectively, and that the identity of the b' state is not presently known.

An experimental curve of growth was constructed for the direct measurement of ground state SnO concentrations. Finally, estimates were made of the system photon yields associated with the Sn + N_2O reaction and of the quenching of the SnO ($a^3\Sigma$) state by (unspecified) flame species. The "system photon yields" reported, ca 0.3% for all SnO electronic transitions, represented the total photon flux emitted from the preheat region of the flame per $SnCl_4$ molecule introduced into the flow. In summary, while the results obtained in these studies were novel and of general interest with regard to possible laser application, they were not sufficiently detailed to permit a fundamental interpretation of the processes occurring in the flames.

The flame studies carried out on the present program represent a continuation and extension of the work briefly outlined. The approach taken was to measure spatial profiles of the metal atom concentrations, the corresponding absolute MO* emissions, and the translational temperature in a number of H_2/N_2O flames having different overall stoichiometries, pressures, and concentrations of metal additives. From these data, fundamental quantitative information was obtained on the quenching of SnO($a^3\Sigma$) and GeO($a^3\Sigma$) within the flames and on the detailed kinetics of the reaction of Sn and Ge with N_2O.

2. APPARATUS AND RELATED HARDWARE

Details of the variable-pressure flame apparatus are given in figure 1. Briefly, the device consists of a large vacuum housing provided with a number of viewing and access ports, a burner (flame holder) on which the flames are stabilized at low pressures, a mechanical vacuum pump which maintains the chamber at a given pressure, and a gas-handling system. To facilitate flame measurements, the burner is mounted on a manipulator so that the flame can be moved with respect to the viewing ports and, therefore, to the optics which are located outside the vacuum housing and which are stationary.

Initial experiments were carried out using a simple unshielded burner, square (4" x 4") in cross section. However, it was quickly recognized that as a consequence of this geometry, both the reaction zone and the chemiluminescent metal oxide emission observed in the preheat region exhibited some curvature along the plane of measurement which complicated the interpretation of the spatial (temporal) measurements. To reduce these flow nonuniformities and also to minimize self-reversal; i.e., the absorption of radiation by cold metal oxide species near the

outer edge of the flame, a large circular porous plate burner was substituted for the more simple device.

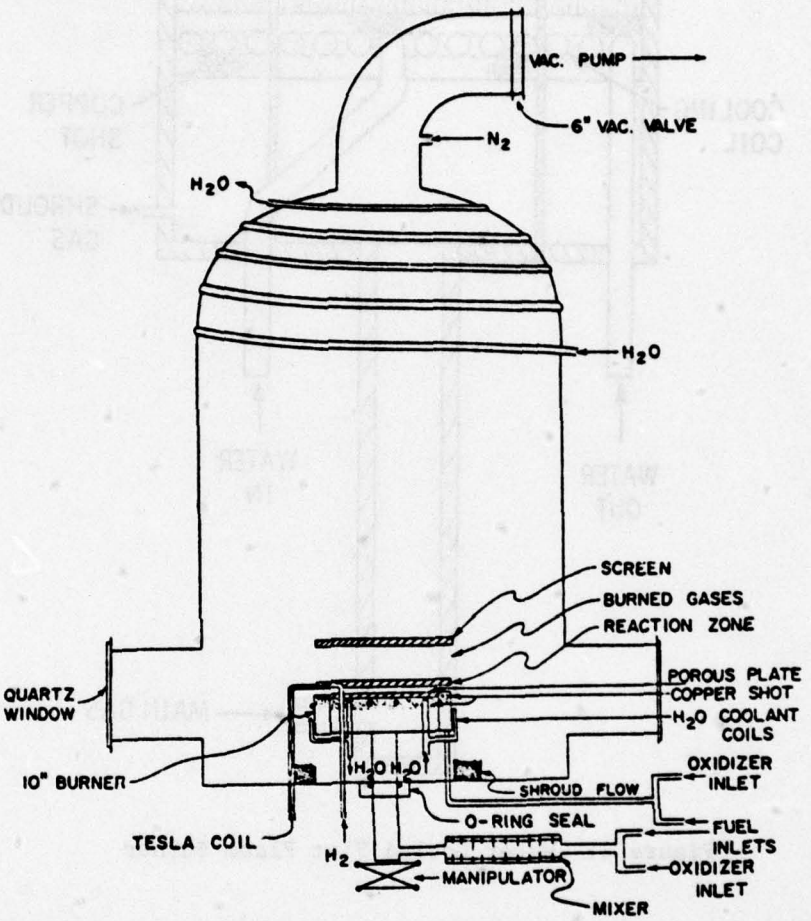

Figure 1. Schematic of the Burner System

A schematic of the porous-plate burner is shown in figure 2. Briefly, the burner is water-cooled and consists of an inner circular portion, 6 inches in diameter, and an outer annular section about 2 inches wide; each section has a separate gas inlet system. In operation, identical flames are supported on each burner, metal compound is added to the inner burner only, and the outer burner provides a shroud flow of hot gases. With this arrangement, it was found that the resulting flames were one-dimensional and the metal oxide chemiluminescent region in the preheat zone was planar and parallel to the burner top.

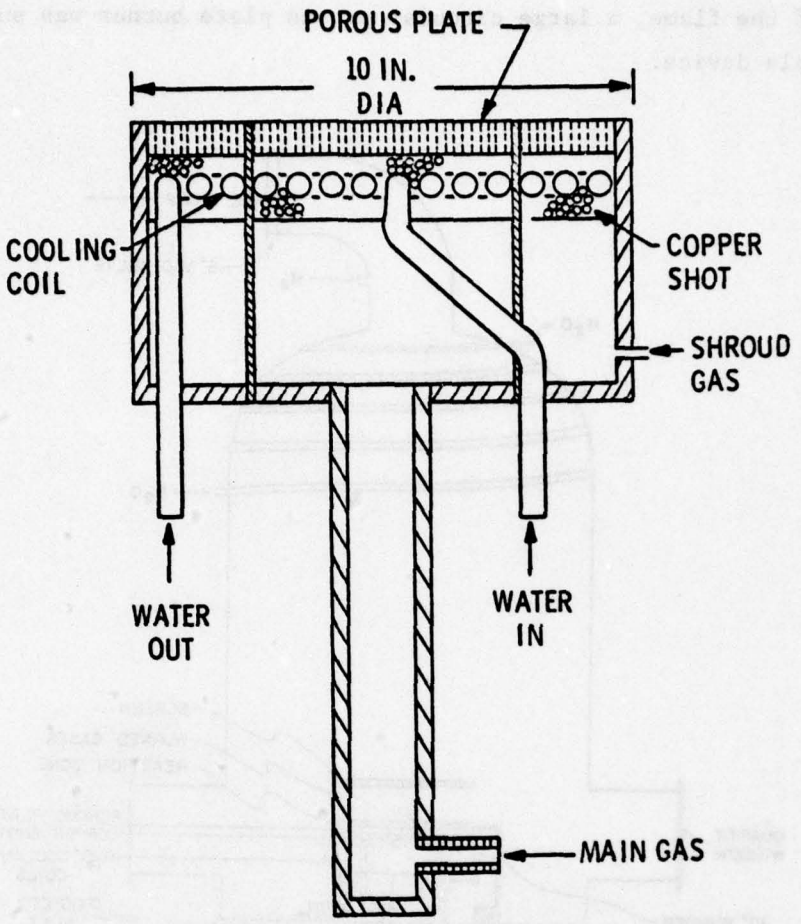

Figure 2. Water Cooled Flat Flame Burner

In all cases, the supply gases (H_2, N_2O and additive for the inner flame) were individually metered (by calibrated critical flow orifices) and thoroughly mixed before entering the burner. Gaseous additives such as SiH_4 were metered and introduced into the unburned flame gases directly from their containing cylinder. A more elaborate metering procedure was required, however, to introduce additives such as $Sn(CH_3)_4$, $SnCl_4$, $GeCl_4$, etc., which are liquids at STP. The method found most convenient for admitting vapors of liquid additives involved a simple transpiration technique in which a fraction of the gases to the inner burner was saturated with additive vapor prior to being mixed into the main flow. The transpiration apparatus consisted of a pyrex cold trap containing glass beads and additive liquid. Known flows of gases, which entered the lower end of the trap and perco-

lated through the beads and liquid to ensure saturation, were withdrawn from the upper section of the trap at a known pressure. The temperature of the cold trap and the vapor pressure of its contents were kept constant throughout the course of an experiment by immersing the trap into either an ice/water slurry or a large container of room temperature water. With this device the flow of vapor was determined by the vapor pressure of the liquid, the flow of gases through the liquid, and the total pressure in the trap which was regulated by a throttle valve located in the exit line.

3. OPTICAL MEASUREMENTS AND ABSOLUTE CALIBRATIONS

Flame spectra were recorded photoelectrically using a Spex Model 1500 monochromator/phase-sensitive (PAR) amplifier combination. For all profile measurements an optical train consisting of a number of lenses and apertures were employed to obtain spatial resolution within the flame volume. Typically, the spatial resolution of the optics was ca 1 mm along the direction of gas flow which for most flames corresponded to a time resolution of about 3×10^{-4} seconds.

Absorption measurements were carried out using a high pressure xenon or a deuterium lamp as a continuous source. Intracavity gain measurements incorporated the use of a Chromabeam Model 1050 Dye Laser and a 2-meter Bausch and Lomb spectrograph.

A standard tungsten iodine lamp of known spectral output was used to obtain the relative system response of the monochromator/detector/window/lens combination over the spectral region $\lambda\lambda$ 3,000-8000Å. The relative response was placed on an absolute basis by permitting light from a blackbody source (Barnes Engineering) to fill the field of view of the optics providing a known calibration signal at a given wavelength.

The metal oxide emission data were placed on an absolute basis in a straightforward manner. The raw spectral data (relative intensity versus λ) recorded for a given location along the flame profile were replotted point-for-point to correct for system response and placed on an absolute basis. The absolute emission for each band system was obtained by spectrally integrating the corrected spectrum with a planimeter. Although this rather laborious procedure was followed to reduce the data from several flames, it was found that a more abbreviated method provided results which were equally reliable. Examination of the spectral data showed that for both GeO and SnO, the transitions making maximum contributions to the total observed absolute intensities were those originating from the $v' = 0$ levels of the

upper electronic states to high v" levels of the ground state. As a result, the spectral distribution of intensities for a given electronic state are not changed appreciably with temperature; i.e., along the flame profile. It was possible, therefore, to obtain the total absolute intensity appropriate to a given electronic transition from a single intensity measurement on a selected vibrational transition. For example, it was found that the integrated band intensity for the SnO(a→X) v' = 0 → v" = 4, 5 or 6 vibrational transitions were proportional to the total integrated intensity as measured by the planimeter. Therefore, for subsequent measurements of total intensity only individual vibrational intensities were required. In general, the agreement between the abbreviated procedures and the planimeter method was within 15%.

4. ATOMIC ABSORPTION CALIBRATIONS FOR Sn AND Ge

Attempts to spectroscopically determine the Sn atom concentrations in a typical H_2/N_2O flame using a narrow line absorption technique (Sn hollow-cathode light source) indicated, that even for very small additions of either $SnCl_4$ or $SnCH_3)_4$, the method was too sensitive and the narrow line source was 100% absorbed. Trials using a continuous source to measure the total absorption or equivalent width, however, proved satisfactory and this method was ultimately employed for all subsequent measurements of atom concentrations in the flames. Since the accurate use of this technique requires the determination of curves of growth (ref. 5) or equivalent calibration curves to relate the measured absorption to the atom concentration, a series of experiments involving the use of a King-type furnace to generate known path lengths and concentrations of Sn and Ge were carried out.

a. Sn Curves of Growth

For the temperatures and pressures for which the absorption measurements are made in the flames, the pressure broadening parameter "a" is expected to be small and, therefore, it is anticipated that the curve of growth for various Sn atom lines will be far from being optically thin. Furthermore, because of the many isotopes of Sn and the resulting complex hyperfine structure, multiple line absorption will take place and an empirical calibration technique must be resorted to to determine atom concentrations from the corresponding absorption measurements. Experimental curves of growth were determined by generating known column densities of Sn atoms by heating tin to various known temperatures in a cell contained in a high temperature carbon tube furnace. The details of construction and use of this

furnace have been described before (ref. 6). Tin pellets were loaded into a small molybdenum boat approximately 8 cm long by 1½ cm wide which was placed in a cylindrical graphite cell approximately 10 cm long by 3 cm in diameter. Graphite end pieces with 6 mm openings were used to confine the metal vapor to a known path length within the graphite cell. The cell was placed in the center of the carbon tube furnace and the apparatus was pressurized with a 50-50 mixture of He and N_2 to conditions of P/T similar to those of the flames. The cell was heated to known temperatures which were measured with a NBS calibrated optical pyrometer. Column densities of Sn atoms within the cell were determined using the vapor pressure data of Honig and Kramer (ref. 7). Absorption measurements were made using a 150 watt high-pressure xenon lamp source and a ½ meter JACO spectrometer equipped with a 1P28 photomultiplier and a PAR HR8 lock-in amplifier. Absorption measurements were made at various temperatures on the 2863Å ($^3P_0 \rightarrow {}^3P_1$), 3009Å ($^3P_1 \rightarrow {}^3P_1$), and the 3175Å ($^3P_2 \rightarrow {}^3P_1$) transitions. Column densities in the various lower states of these transitions were calculated from the known vapor pressures and lower state excitation energies assuming a Boltzmann distribution.

Typical results are shown in figure 3 in which total absorptions for the various transitions versus column density is given at a P/T (torr/°K) of approximately .012. The information shown in this figure can be combined into a single curve of growth by replotting the various total absorptions against the quantity $Nf\ell$ which represents the product of the column density and the oscillator strength of the particular transition (ref. 5). Using the oscillator strengths given by Penkin and Slavenas (ref. 8); i.e., $f_{2863} = .230$, $f_{3009} = .059$, and $f_{3175} = .105$, the curve of growth shown in figure 4 is obtained. It should be noted that for very small absorptions, as expected, the total absorption has a linear dependence on $Nf\ell$ whereas for very large absorptions it approaches the expected square root dependency. As anticipated, this curve of growth is far from being optically thin and a very rough estimate of the pressure broadening parameter was found to be approximately .05.

With these results it becomes possible to inventory the densities of Sn not only in its ground electronic state ($^3P_0$) but also in the $^3P_1$ and $^3P_2$ excited levels.

b. Ge Curves of Growth

Curves of growth for a P/T value of approximately 0.014 torr/°K have been measured for the GeI ground state transitions, $^3P_0 \rightarrow 5S{}^3P_1$, $^3P_2^0 \rightarrow 5S{}^3P_2^0$, and

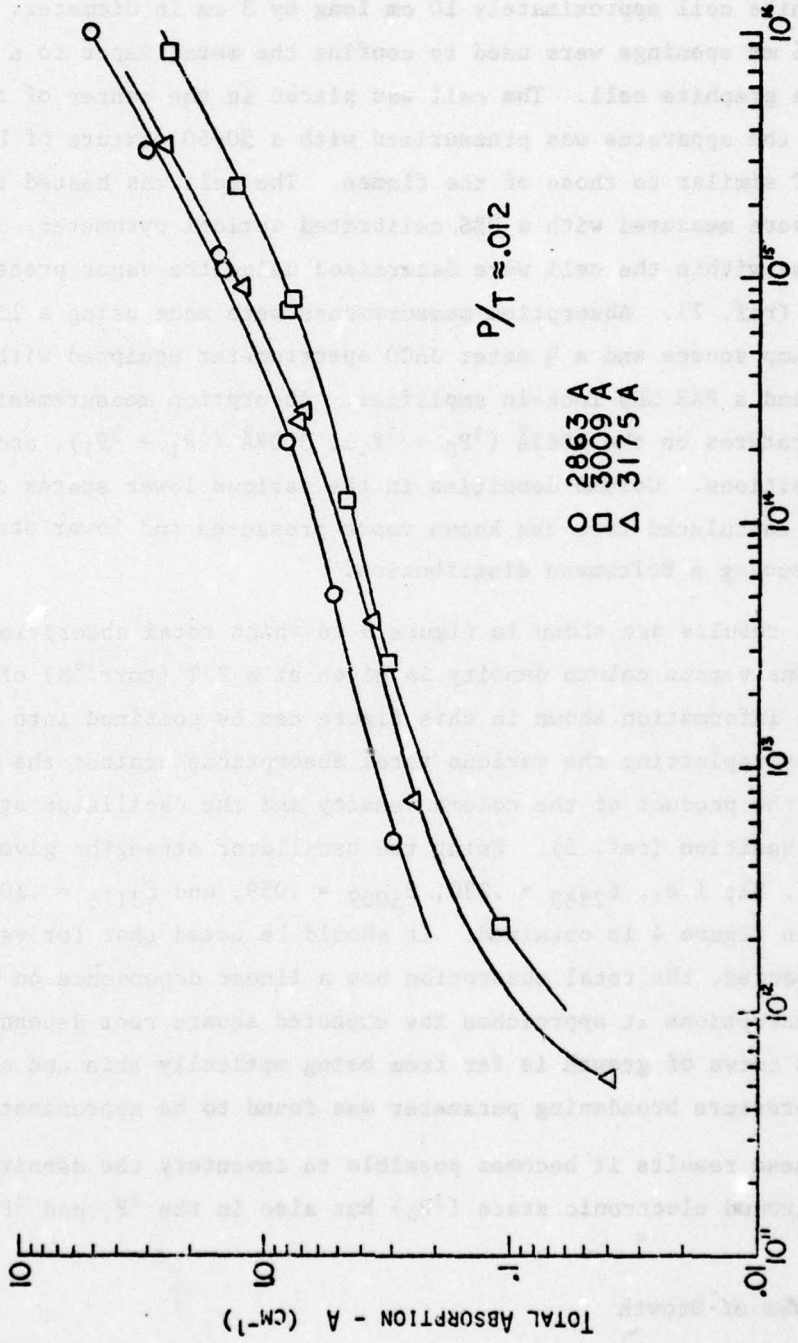

Figure 3. Total Absorption for SnI 2863Å, 3009Å, and 3175Å Lines as a Function of Column Densities. P/T - .012

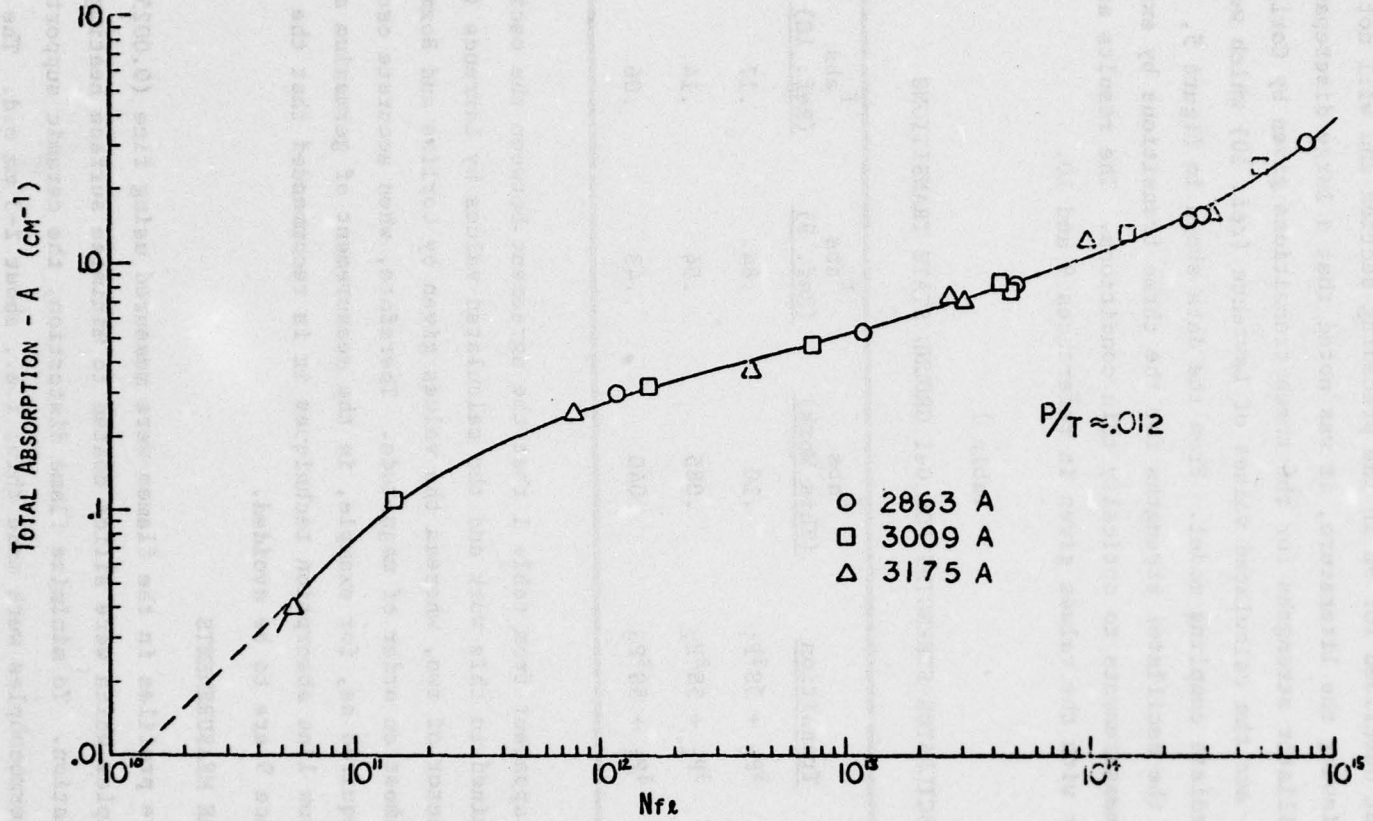

Figure 4. Curve of Growth for SnI. P/T ≈ .012

$^3P_1 \rightarrow 5S^3P_0^0$ at 2651.58Å, 2651.18Å, and 2709.63Å. The method employed was entirely analogous to that described for Sn in the preceding section and will not be repeated. In reviewing the literature, it was noted that a large discrepancy exists between the oscillator strengths for the three transitions given by Corliss and Bozman (ref. 9), and the calculated values of Lawrence (ref. 10) which were obtained using an intermediate coupling model. From the data shown in figure 5, it was possible to obtain the oscillator strengths for the three transitions by extrapolating the absorption measurements to optically thin conditions. The results are shown in Table 1 together with the values given in references 9 and 10.

Table 1

OSCILLATOR STRENGTHS FOR GeI GROUND STATE TRANSITIONS

λ_A	Transition	f_{abs} (This Work)	f_{abs} (Ref. 9)	f_{abs} (Ref. 10)
2651.59	$^3P_0 \rightarrow 5S^3P_1$	.10	.84	.17
2651.18	$^3P_2 \rightarrow 5S^3P_2$	.085	.54	.14
2709.63	$^3P_1 \rightarrow 5S^3P_0$	.040	.43	.06

It is apparent from table 1 that the agreement between the oscillator strengths determined in this work and the calculated values by Lawrence (ref. 10) is well within a factor of two, whereas the values given by Corliss and Bozman appear to be high by almost an order of magnitude. Therefore, when accurate oscillator strengths are required as, for example, in the measurement of germanium atom concentrations by narrow line absorption techniques it is recommended that the values given in reference 9 are to be avoided.

5. TEMPERATURE MEASUREMENTS

Temperature profiles in the flames were measured using fine (0.0025 cm) Pt/Pt-10% Rh thermocouples which were silica coated to minimize surface heating by free radical recombination. To minimize flame distortion, the ceramic supporting structures for the thermocouples were made thin; i.e., about 2-3 mm o.d. The thermocouples were inserted into the flames with their lengths parallel to the burner top and their location relative to that surface was accurately measured with a cathetometer.

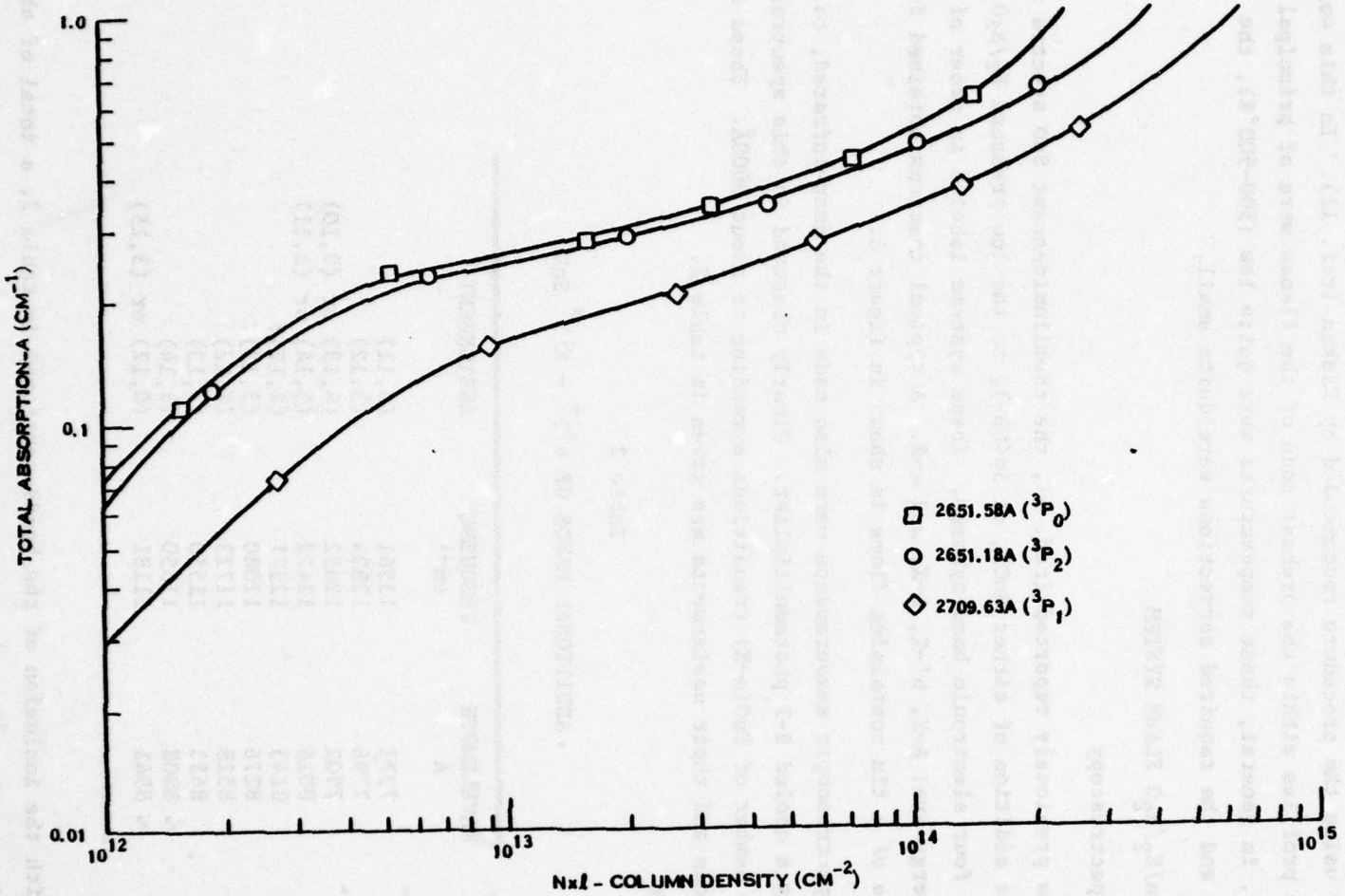

Figure 5. Germanium Curves of Growth. P/T = .014

In reducing the thermocouple data, observed temperatures were corrected for radiation losses using the procedure recommended by Kaskan (ref. 11). In this work, the temperature profiles within the preheat zone of the flames were of principal interest. Since, in general, these temperatures were quite low (500-900°K), the radiation losses and the required corrections were quite small.

6. THE $Sn/H_2/N_2O$ FLAME SYSTEM

a. Spectroscopy

As previously reported (ref. 1), the chemiluminescent SnO spectra resulting from the addition of either $SnCl_4$ or $Sn(CH_3)_4$ to the low pressure H_2/N_2O flames consists of four electronic band systems. These systems labeled in order of decreasing energy are: A→X, b'→X, b→X, and a→X. A typical spectrum obtained from the preheat zone of a tin containing flame is shown in figure 6.

Spectroscopic measurements were also made in the near-infrared, to about 1.1 μ, using a cooled S-1 photomultiplier. Clearly observed in this spectral region were a number of SnO(a→X) transitions extending to about 9000Å. These newly measured bands and their assignments are given in table 2.

Table 2

ADDITIONAL BANDS OF $a^3\Sigma^+ \rightarrow X^1\Sigma^+$ SnO

WAVELENGTH A	FREQUENCY cm^{-1}	ASSIGNMENT
7372	13561	(3,11)
7796	12824	(3,12)
7902	12652	(4,13) or (0,10)
8016	12472	(5,14) or (1,11)
8143	12277	(2,12)?
8276	12080	(3,13)?
8528	11723	(1,12)
8656	11550	(2,13)
∿ 8808	11350	(3,14)
∿ 8941	11181	(0,12) or (3,15)

With the inclusion of the bands contained in table 2, a total of about 31 band heads for the $a^3\Sigma \rightarrow X^1\Sigma$ systems of SnO were fit to the equation (ref. 1).

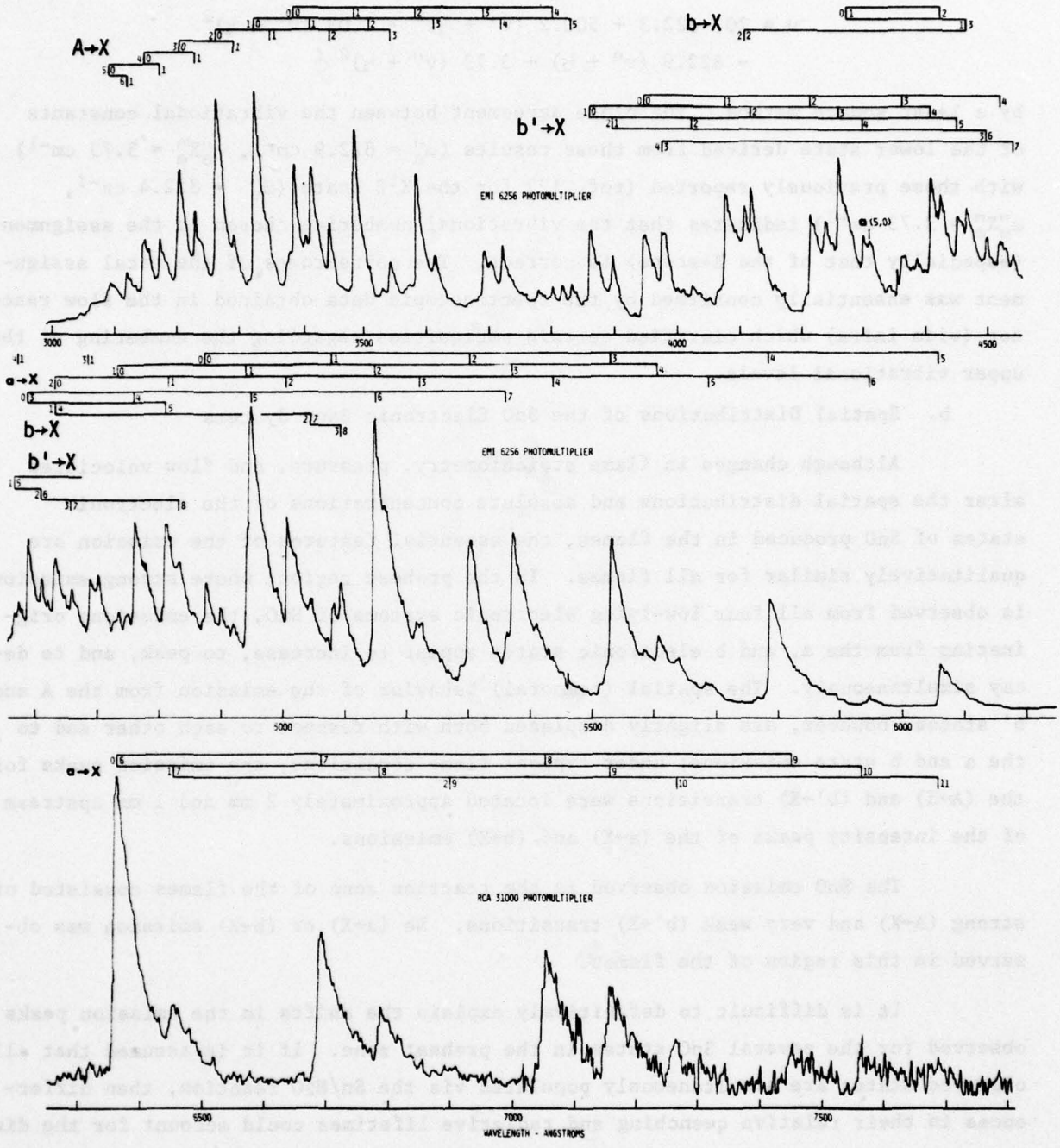

Figure 6. $SnCl_4/H_2/N_2O$ Chemiluminescence Flame Spectra (Uncorrected for Detector Response)

$$\nu = 20,\ 622.3 + 500.2\ (v' + \tfrac{1}{2})^2 - 1.03\ (v' + \tfrac{1}{2})^2$$
$$- 822.9\ (v'' + \tfrac{1}{2}) + 3.73\ (v'' + \tfrac{1}{2})^2$$

by a least square method. The close agreement between the vibrational constants of the lower state derived from these results (ω_e'' = 822.9 cm^{-1}, $\omega_e''x_e''$ = 3.73 cm^{-1}) with those previously reported (ref. 12) for the $X^1\Sigma$ state (ω_e'' = 822.4 cm^{-1}, $\omega_e''x_e''$ = 3.73 cm^{-1}) indicates that the vibrational numbering chosen in the assignment (especially that of the X-state) is correct. The correctness of the total assignment was essentially confirmed by the spectroscopic data obtained in the flow reactor (vide infra) which clarified certain ambiquities regarding the numbering of the upper vibrational levels.

b. Spatial Distributions of the SnO Electronic Band Systems

Although changes in flame stoichiometry, pressure, and flow velocities alter the spatial distributions and absolute concentrations of the electronic states of SnO produced in the flames, the essential features of the emission are qualitatively similar for all flames. In the preheat region, where strong emission is observed from all four low-lying electronic systems of SnO, the emissions originating from the a, and b electronic states appear to increase, to peak, and to decay simultaneously. The spatial (temporal) behavior of the emission from the A and b' states, however, are slightly displaced both with respect to each other and to the a and b state emissions; under typical flame conditions, the emission peaks for the (A→X) and (b'→X) transitions were located approximately 2 mm and 1 mm upstream of the intensity peaks of the (a→X) and (b→X) emissions.

The SnO emission observed in the reaction zone of the flames consisted of strong (A→X) and very weak (b'→X) transitions. No (a→X) or (b→X) emission was observed in this region of the flames.

It is difficult to definitively explain the shifts in the emission peaks observed for the several SnO states in the preheat zone. If it is assumed that all observed states are simultaneously populated via the Sn/N_2O reaction, then differences in their relative quenching and radiative lifetimes could account for the displacements. For example, if the radiative lifetimes of the a and b states are appreciably longer than those for A and b', quenching of the emission along the flame profile will be more important for the former; alternatively, the short-lived A and b' states can emit radiation very shortly after they are formed and before they are appreciably quenched. This effect can easily account for the small spatial shifts.

However, because of the complex nature of the flame kinetics and the relatively high spatial resolution required for a detailed study of these small shifts, it was felt that a thorough investigation of these effects would best be deferred for a future study.

As discussed previously, the emission observed in the reaction zone of the flames results from radical recombination on SnO species. Since the transition probabilities for the (A→X) transitions are known to be very large, and the observed intensities for the b'→X transitions were very weak, the absolute concentrations of SnO* (A and b') present in this region of the flame are small and the mechanisms producing the excitations are, therefore, inefficient and not of direct interest with regard to laser chemistry.

The primary species of interest in the flames is $SnO(a^3\Sigma)$. Therefore, the major portion of the experimental work was directed towards the study of its kinetics and to detailed measurements of its temporal behavior in the flame gases.

c. Kinetics

The kinetics of SnO* formation and deactivation can be described in terms of the following kinetic sequence:

$$Sn + N_2O \xrightarrow{k^*} SnO^* + N_2 \quad (1)$$

$$Sn + N_2O \xrightarrow{k} SnO + N_2 \quad (2)$$

$$SnO^* + M \xrightarrow{k_Q} \text{Products} \quad (3)$$

$$SnO^* \xrightarrow{A} SnO + h\nu \quad (4)$$

where k* is the rate constant for the production of excited species, k is the rate constant for the production of nonradiating species, and k_Q and A are, respectively, the rate constant for quenching of SnO* by a species M, and the transition probability for a given electronic state. Note that this description of the kinetics of formation of SnO is "global" in that it assumes that the rate constants k* and k are identical for all electronic states of Sn. From reactions (1-4) it follows that

$$\frac{d(SnO^*)}{dt} = k^*[Sn][N_2O] - (A + k_Q[M])[SnO^*] \quad (5)$$

Since the rate constant k* is equal to the total rate constant for the Sn/N_2O reaction ($k_T = k^* + k$) multiplied by the branching ratio ϕ_o, and the intensity of a given SnO* transition is given by:

$$I = A[SnO^*] \tag{6}$$

it is easy to show that equation (5) can be rewritten as

$$\frac{1}{A}\frac{d\ln I}{dt} = \frac{\phi_o k_T[Sn][N_2O]}{I} - (1 + k_Q[M]/A) \tag{7}$$

In the experiments to be described, the Sn atom concentration, the flame kinetic temperature and the absolute intensity, I, of the ($a^3\Sigma$) transitions were measured at several locations within the preheat zones of a number of flames. These data were then reduced to obtain photon yields, ϕ, for each point along the flame profile. The photon yield for a given transition and location within the flame is by definition the ratio of the number of photons emitted per reactive event, and can be written as

$$\phi = \frac{I}{k_T[Sn][N_2O]} \tag{8}$$

In obtaining photon yields, k_T was evaluated using an average value for the rate constant of the Sn/N_2O determined by Felder and Fontijn (ref. 2); i.e.,

$$k_T = 10^{-11}\, e^{-3000/T}\ cm^3/molecule\ sec \tag{9}$$

Substitution of equation (8) into equation (7) yields the result:

$$\frac{1}{A}\frac{d\ln I}{dt} = \frac{\phi_o}{\phi} - 1 - \frac{k_Q[M]}{A} \tag{10}$$

It is of interest to examine the properties of equation (10). For fully allowed transitions (large values of A) $\phi/\phi \approx 1$. Therefore, for states with sufficiently short radiative lifetimes (e.g., $A(^1\Pi)$) the photon yield is insensitive

to quenching and the emission at all locations along a profile in the preheat zone is collision-limited; i.e.

$$I = \phi_o k_T [Sn][N_2O] \tag{11}$$

For electronic species having long radiative lifetimes, the time variations of the intensity along the profile (equation 10) is a complex function of both the radiative lifetimes and the quenching parameters.

Within the preheat zone, each SnO* intensity profile achieves a maximum value. At this location, $d\ln I/dt = 0$, the system approaches steady-state ($d[SnO^*]/dt = 0$), and

$$\phi = \frac{\phi_o}{1 + k_Q[M]/A} \tag{12}$$

Rewritten in terms of more fundamental prarmeters, equation (12) becomes:

$$I = \frac{\phi_o k_T [Sn][N_2O]}{1 + k_Q[M]/A} \tag{13}$$

Therefore, for a given flame, assuming that the addition of tin species does not change the flame temperature or the quenching, the peak emission intensity varies simply as [Sn].

The kinetic model, equations (1-4), formally assumes a single quenching reaction. If a number of species contribute to SnO* quenching, the simple parameters $k_Q[M]/A$ must be replaced by the summation: $\sum_i k_{Q_i}[M_i]$.

In the experimental work to be discussed, it was found that the behavior of the $SnO(a^3\Sigma)$ intensities in a number of flames could be correlated in terms of the kinetic model described, and from an analysis of the data, it was possible to obtain fundamental information regarding its formation and quenching by flame species.

d. Interpretation of the $SnO(a^3\Sigma)$ Profile Measurements

Initial experiments to determine the maximum concentrations of $SnO(a^3\Sigma)$ that could be produced in the H_2/N_2O flames were carried out using either $SnCl_4$ or

$Sn(CH_3)_4$ as additives. For both materials, the results obtained were substantially the same. Briefly, it was found that for any given flame, the absolute concentration of $SnO(a^3\Sigma)$ appeared to approach a maximum value as greater concentrations of tin compounds were added to the flame, and that further increases in the concentration of additive did not produce corresponding increases in $SnO(a^3\Sigma)$. Unfortunately, it was also found impossible to increase the concentration of $SnO(a^3\Sigma)$ to the levels required for lasing by changing the flame pressure, stoichiometry, and additive concentrations although extensive efforts to optimize all three were carried out. As a result of these observations, a series of detailed profile measurements were made to gain information on the limiting processes.

Profile data for five typical flames are summarized in table 3. Contained in the listings are: the absolute $SnO(a\rightarrow X)$ intensities, the measured $Sn(^3P_0)$ and $(^3P_1)$ concentrations and the corresponding electronic tin temperatures, T_{elect}; the temperatures measured by thermocouple, T_{kin}; and the calculated H_2, N_2O, and total (all states) tin atom concentrations. The N_2O and H_2 concentrations in the preheat region were computed from the known gas composition, the local (kinetic) flame temperature, and the total pressure, assuming that no substantial combustion had occurred. The total tin concentrations were obtained using the measured $Sn(^3P_0)$ concentrations and the relation

$$Sn_T = Sn(^3P_0)Q_e \qquad (14)$$

where, Q_e, the electronic partition function, was evaluated using the (local) measured T_{elect}. Also shown in the table are the photon yields, ϕ, at several locations along the flame profiles obtained using equation (8).

The data in the table show several important features. For all flames, regardless of the additive used, the electronic tin temperature is observed to first increase with distance from the burner top, to achieve a peak value, and to then fall-off gradually at greater distances. Since the translational (kinetic) temperature of the flame increases monotonically with distance, the measurements clearly indicate a lack of close coupling between the electronic and translational temperatures in the flames. In general, it was also found that for a given flame, the peak T_{elect} obtained using $Sn(CH_3)_4$ as additive was somewhat higher than that for $SnCl_4$.

Table 3.

PROFILE DATA ON H_2/N_2O/He FLAMES WITH Sn ADDITIVE

RUN	Z mm	Time x 10^4 sec	$I_{a \rightarrow X}$ x 10^{-13} Ph/cc/sec	[Sn $^3P_0$] x 10^{-12}	[Sn $^3P_1$] x 10^{-12}	[Sn_{Tot}] x 10^{-12}	Temperature Electronic °K	Temp Kinetic °K	[N_2O] x 10^{-16}	[H_2] x 10^{-16}	ϕ
P = 15.0 torr	1	5.4	5.32	.55	.14	.70	988	460	7.5	9.8	.068
H_2/N_2O = 1.3	2	9.5	15.8	.85	.35	1.27	1227	580	5.9	7.7	.037
	3	12.8	22.5	.92	.37	1.36	1212	730	4.7	6.1	.021
$Sn(CH_3)_4$	4	15.4	20.4	.72	.39	1.21	1423	880	3.9	5.1	.013
	5	17.6	13.6	.45	.28	.82	1548	1020	3.4	4.4	.0092
	6	19.6	6.11	.20	.12	.36	1513	1160	3.0	3.9	.0075
	7	21.3	2.76	.12	.089	.24	1743	1280	2.7	3.5	.0044
	8	22.9	1.58	.12	.085	.24	1688	1390	2.5	3.3	.0022
	9	24.4	1.30	.13	.089	.25	1649	1490	2.3	3.0	.0017
	10	25.8	1.18	.16	.11	.31	1653	1570	2.2	2.9	.0012
	1	5.5	1.58	.95	.13	1.09	789	380	5.6	18.5	.070
P = 9.5 torr	2	10.3	3.51	1.0	.16	1.17	831	415	5.2	17.1	.079
	3	14.7	5.54	1.1	.17	1.24	832	460	4.6	15.2	.064
H_2/N_2 = 3.3	4	18.7	6.93	1.0	.20	1.23	893	510	4.2	13.9	.048
	5	22.3	7.53	.87	.21	1.10	969	565	3.8	12.5	.037
$Sn(CH_3)_4$	6	25.5	6.78	.62	.19	.84	1068	635	3.4	11.2	.027
	7	28.4	5.66	.46	.16	.67	1130	700	3.1	10.2	.020
	8	31.0	4.31	.30	.13	.45	1259	760	2.8	9.2	.018
	9	33.4	2.84	.21	.093	.32	1273	825	2.6	8.6	.013
	10	35.6	1.73	.12	.054	.18	1284	885	2.4	7.9	.012
	11	36.7	.95	.10	.042	.15	1239	940	2.3	7.6	.0067
	12	38.7	.16	.067	.037	.11	1440	1000	2.1	6.9	.0048

(continued)

Table 3

Profile Data on H_2/N_2O/He Flames with Sn Additive

RUN	Z mm	Time x 10^4 sec	I a→X x 10^{-13} Ph/cc/sec	[Sn $^3P_0$] x 10^{-12}	[Sn $^3P_1$] x 10^{-12}	[Sn] x 10^{-12}	Temp. Electronic °K	Temp. Kinetic °K	[N_2O] x 10^{-16}	[H_2] x 10^{-16}	ϕ
P = 9.8 Torr	2	7.8	5.17	.55	.17	.75	1070	430	5.6	7.3	.13
H_2/N_2O = 1.3	3	11.2	10.2	.68	.26	.98	1183	510	4.7	6.1	.079
	4	13.1	12.2	.55	.33	.98	1514	660	3.6	4.7	.031
$Sn(CH_3)_4$	5	15.3	10.0	.35	.24	.68	1651	850	2.8	3.6	.018
	6	17.1	5.86	.27	.18	.52	1620	980	2.45	3.2	.0098
	7	18.9	2.70	.12	.08	.23	1620	1060	2.3	3.0	.0087
	8	20.4	1.20	.06	.035	.11	1566	1120	2.15	2.8	.0074
P = 9.8 Torr	1	4.4	3.55	.62	.16	.80	993	400	6.0	6.0	.13
H_2/N_2O = 1.3	2	7.5	8.87	1.11	.33	1.49	1054	430	5.6	7.3	.11
	3	10.8	14.6	1.23	.47	1.78	1182	510	4.7	6.1	.062
$Sn(CH_3)_4$	4	12.7	18.8	1.26	.51	1.86	1216	660	3.6	4.7	.026
	5	14.8	18.8	1.04	.55	1.74	1404	850	2.8	3.6	.013
	6	16.5	15.1	.72	.45	1.32	1553	980	2.45	3.2	.010
	7	18.2	16.4	.52	.35	1.00	1630	1060	2.3	3.0	.0078
	8	19.7	5.52	.29	.19	.55	1601	1120	2.15	2.8	.0068
	9	21.1	2.17	.15	.085	.26	1462	1170	2.1	2.7	.0053
P = 9.2 Torr	2	7.3	5.11	.62	.24	.89	1190	430	5.3	6.9	.12
	3	10.5	8.40	.70	.30	1.06	1252	510	4.4	5.7	.060
H_2/N_2O = 1.3	4	12.4	7.96	.47	.20	.71	1250	660	3.4	4.4	.030
	5	14.4	5.07	.22	.11	.36	1360	850	2.6	3.4	.018
$SnCl_4$	6	16.1	2.32	.15	.057	.21	1175	980	3.0	3.0	.010
	7	17.7	1.16	.10	.033	.14	1103	1060	2.9	2.9	.0066

The observation that a small degree of chemiexcitation exists for the $Sn(^3P_1)$ level is not completely anomolous. For example, it has been found (ref. 1) that the addition of very small quantities of CCl_4 to an $H_2/N_2O/SnCl_4$ flame can give rise to strong Sn line emission in the preheat zone, and chemiluminescence from Sn lines with energies up to 50,000 cm^{-1} could be detected. For these experiments it was suggested that energy exchange between vibrationally or electronically excited CO could populate very high electronic states of Sn. In the present experiments, it is possible that the interactions of additive fragments with flame species can lead to superthermal population of the $^3P_1$ state of Sn.

Perhaps the most important feature of the data is the fact that the photon yields, ϕ, for each of the flames are initially quite high but rapidly decrease with time indicating quenching of $SnO(a^3\Sigma)$ along the flame profile. It is also interesting to note the fact that near the peak of the $SnO(a\rightarrow X)$ emission in any given flame, the emission appears to be proportional to $[Sn_T]$ and virtually independent of the rapidly changing temperature profile. This behavior suggests, as will be shown, that the temperature dependence of the rate constant for $SnO(a^3\Sigma)$ quenching is nearly identical with that for the production of $SnO(a^3\Sigma)$ by the Sn/N_2O reaction.

Employing the results of the kinetic analysis presented in paragraph c, the profile measurements were used together with equation (7) to obtain a measure of the quenching parameter $k_Q[M]/A$ at each point along the flame profiles.

In reducing the data, values for $d\ln I/dt$ at each point along a given flame profile were obtained graphically from plots of $\ln I$ versus time, and the corresponding photon yields were calculated using equation (8). For all calculations, it was assumed that $A(SnO(a^3\Sigma)) = 10$ /sec (ref. 13), and that $\phi_o = 0.5$. The value adopted for the branching ratio, 0.5, is consistent with the experimental results on $SnO(a^3\Sigma)$ formation reported by Felder and Fontijn (ref. 2) and is also compatible with the flame profile data. Concerning the latter, it may be worth noting that if it is assumed that at early times along the flame profile, $k_Q[M]/A$ is very small, it becomes possible to estimate ϕ_o using equation (7). For all five flames contained in table 3, values of ϕ_o obtained ranged between 0.4 and 0.5.

The quenching parameters, $k_Q[M]/A$, calculated for the five profiles are shown in figure 7. From these data it is obvious that the effects of quenching, while relatively small at early times along the flow, can severely limit the absolute concentrations of $SnO(a^3\Sigma)$ which can be achieved in the downstream gases and, therefore, reduce the photon yields to the low values observed at longer times.

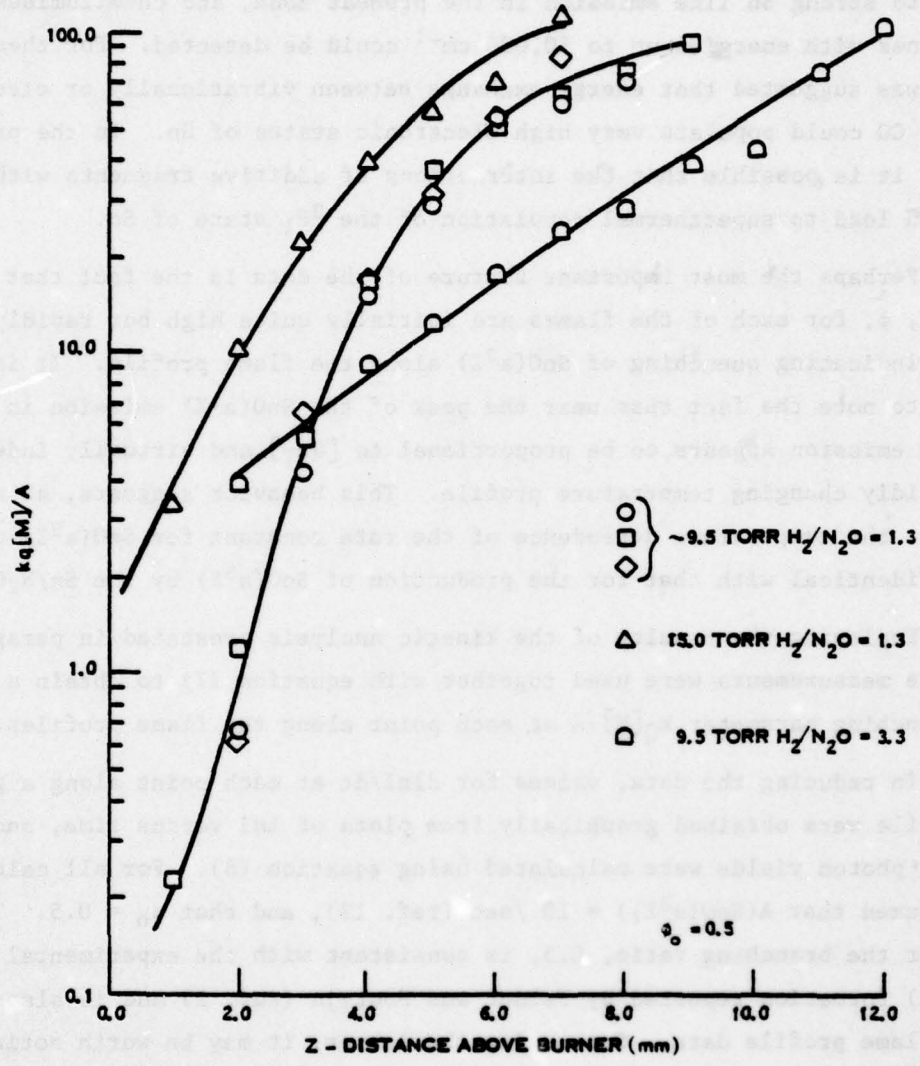

Figure 7. Quenchant Parameter as a Function of Flame Position

If it is assumed that the measured quenching parameters in figure 7, result from a process such as

$$SnO(a^3\Sigma) + M \xrightarrow{k_Q} \text{Products} \qquad (15)$$

where the rate constant k_Q is a constant for a given flame, then the increase of $k_Q[M]/A$ with distance (time) can be attributed to increases in the quenchant species concentration along the profile. Since the maximum value of $k_Q[M]/A$ measured in the flames was about 100, then if $k_Q \sim 10^{-10}$ cm^3/molecule sec (gas kinetic), the minimum [M] required to account for the observed quenching at long times is ca 10^{15}/cm^3. Therefore, it appears that tin species present in the flames cannot be the major quenchants since their maximum concentrations in the flame are determined by the additive flow and do not exceed 10^{14}/cm^3. The possibility that combustion products such as H_2O, and O_2 are dominant quenchants was eliminated (vide infra) in separate experiments in which it was found that they do not substantially quench $SnO(a^3\Sigma)$. While quenching by flame free-radicals cannot be positively ruled out, it is unlikely that their concentrations in the preheat zone can be large enough (greater than 10^{15}/cm^3) to affect quenching.

An alternative, and as it turns out, much more satisfactory explanation involves the assumption that the quenchant concentration in the flame is virtually constant and that the variation in the quenching parameter is the result of a temperature dependent quenching rate constant. If it is assumed that [M] = N_2O it is possible to obtain the value of k_Q appropriate to each point in the flames using the data in figure 7, and to determine the temperature dependence of the rate constant from a plot of log k_Q vs. $1/T_{kin}$. The results of this procedure show that the data for four of the five flames lie on a common straight line; however, the data from the flame containing the greatest hydrogen concentration appears to lie on a line slightly displaced from that of the other four. Furthermore, the value of the resulting rate constant which must be associated with N_2O quenching obtained in this manner is found to be much greater than the value (10^{-14}) reported by Felder and Fontijn (ref. 2).

If it is assumed that [M] = H_2, the data for all flames, figure 8, coalesce on a common straight line and are satisfactorily correlated. On the

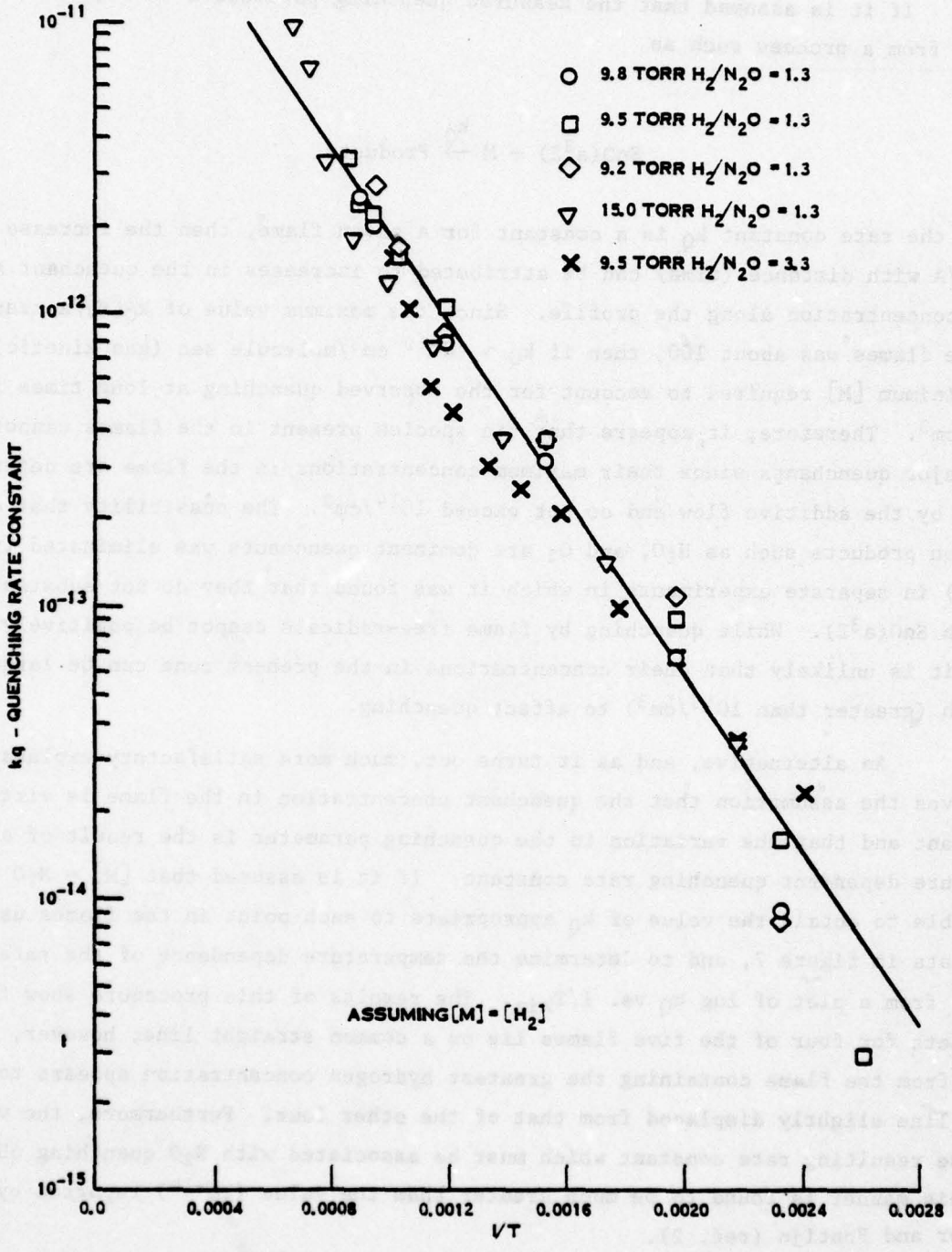

Figure 8. Temperature Dependence of k_Q; [M] = H_2

strength of this evidence, it would appear that the most probable quenchant of $SnO(a^3\Sigma)$ in the flame is molecular hydrogen. The rate constant for this process is found to be given by

$$k_Q = 5 \times 10^{-11} \exp(-3400/T) \text{ cm}^3/\text{molecule sec} \qquad (16)$$

In order to seek confirmation on H_2 quenching, an additional set of experiments was designed to extend the variation of $[H_2]$ over that of the flames for which the detailed profiles were measured. In these experiments the peak $SnO(a \rightarrow X)$ intensity and the corresponding Sn atom concentration and kinetic temperature were measured in six flames having different (unburned) hydrogen and N_2O concentrations.

The data obtained for the flames are summarized in table 4. An interesting aspect of these data is that although the H_2 concentration in the flames was varied over a fairly broad range, the kinetic temperature in the region of peak $SnO(a \rightarrow X)$ emission (measured by thermocouple) is virtually the same for all flames. Although the small temperature variation for these data precludes confirmation of the temperature dependence of the quenching constant, the fact that the temperature can be considered constant considerably simplifies the analysis of the data.

Table 4
HYDROGEN QUENCHING AT PEAK OF PROFILE

FLAME NO.	T_{kin} PEAK °K	T_{elec} PEAK °K	$I_{(a \rightarrow X)} \times 10^{-14}$ ph/cc/s	$[Sn]_{TOT} \times 10^{-12}$ /cc	$[N_2O] \times 10^{-16}$ /cc	$[H_2] \times 10^{-16}$ /cc	$k_Q[M]/A$
1	675	1042	1.37	2.05	3.14	10.5	26.5
2	700	1117	1.76	1.64	3.59	9.52	22.1
3	690	1360	1.56	1.05	4.12	7.08	16.9
4	670	1306	1.95	1.01	3.29	3.71	8.71
5	664	1343	2.01	1.07	3.80	4.95	10.0
6	630	1000	1.45	.84	4.76	4.84	10.8

Recalling that (eq. 13)

$$I \text{ peak} = \frac{k_T \phi_o [Sn][N_2O]}{1 + k_Q[M]/A}$$

it is possible to obtain the quantity $k_Q[M]/A$ since k_Q, [Sn], I peak, and $[N_2O]$ are directly measured or calculated quantities. This procedure was used to measure the quenching parameters for the data in table 4; the resulting values of $k_Q[M]/A$ are shown plotted against the hydrogen concentrations in figure 9. From these data it was possible to obtain a value of 2.4×10^{-13} cc/molecule sec for the quenching constant at T = 670 °K. This value is in excellent agreement with that obtained from equation (16). It is felt that these results clearly confirm that H_2 is the dominant quenchant for $SnO(a^3\Sigma)$.

While there is no doubt that H_2 quenches $SnO(a^3\Sigma)$, the detailed nature of the process is not known. The rather substantial activation energy associated with k_Q, 6.8 kcal/mole, suggests that H_2 may be reacting chemically to remove $SnO(a^3\Sigma)$. The activation energy associated with the quenching rate constant also explains the apparent insensitivity to temperatures of the $I(a \rightarrow X)$ intensities near the region of peak emission in the flames.

In summary, the quenching of $SnO(a^3\Sigma)$ by H_2 in the flames satisfactorily explains the overall behavior of the emission profiles measured for this species. Unfortunately, since H_2 is a major flame component, it was not possible to substantially reduce $[H_2]$, minimize quenching, and to simultaneously achieve stable burning conditions. A number of hydrogen and nonhydrogen containing fuels such as C_2H_2, CH_4, C_2N_2 and others were burned with N_2O in attempts to find an alternative nonquenching flame system. These attempts were not successful. As will be seen from the flow reactor studies, these species also appear to substantially quench $SnO(a^3\Sigma)$.

e. Limitations of $SnO(a^3\Sigma)$ Production

Having explained the essential features of the profiles, attention was next focussed on the study of processes such as self-quenching and tin atom depleting reactions which could potentially lead to the limited concentrations of $SnO(a^3\Sigma)$ produced in the flames. In the context of this report, self-quenching refers to the quenching of $SnO(a^3\Sigma)$ by SnO_x species present in the flame.

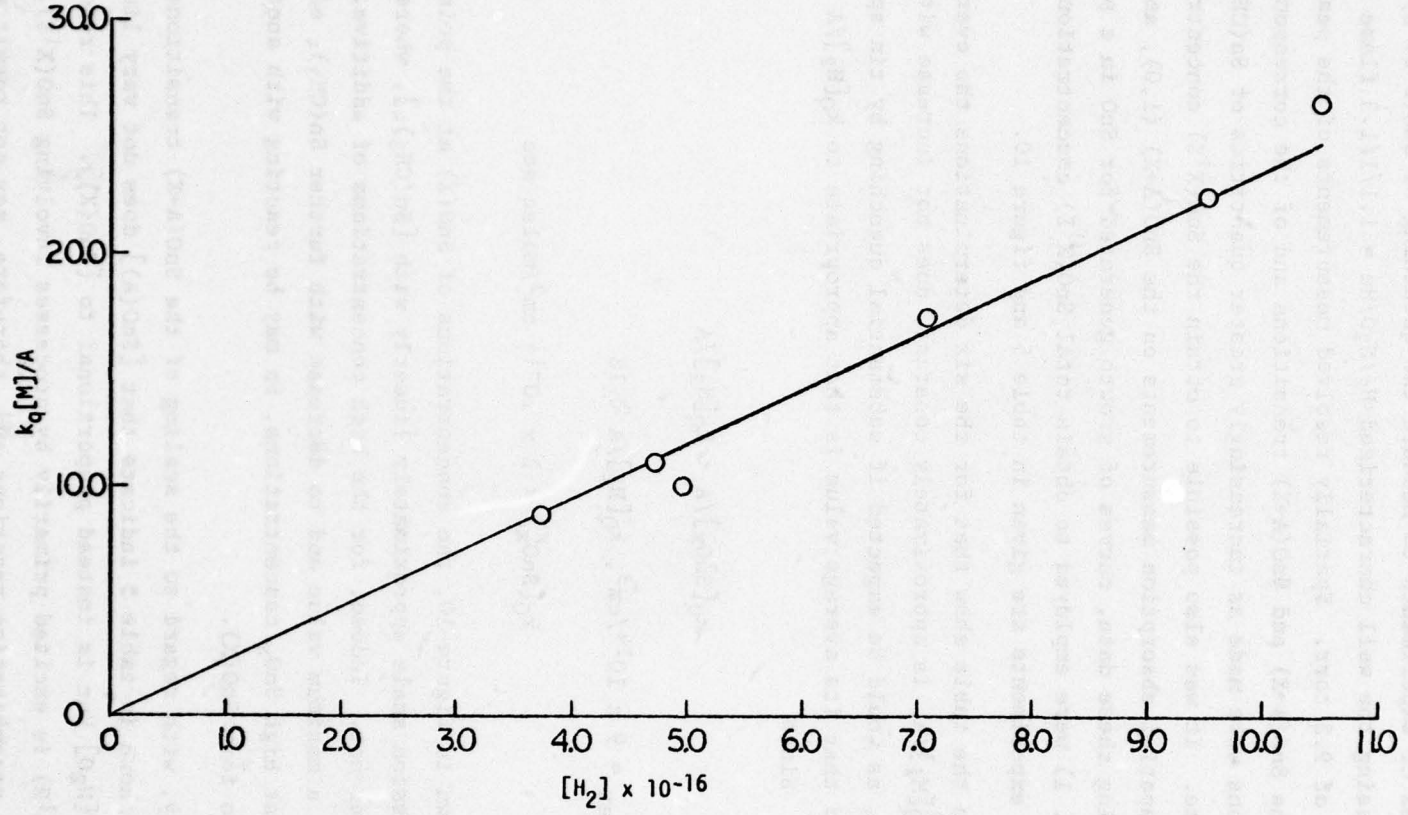

Figure 9. Variation of Quenching Parameter with $[H_2]$

A series of experiments to measure the quenching of $SnO(a^3\Sigma)$ by SnO was carried out using the well characterized $H_2/N_2O/He$ = 1.1/1/1.3 flame burned at a total pressure of 9.5 torr. Spatially resolved measurements of the peak absolute intensities of the SnO(a→X) and SnO(A→X) transitions and of the corresponding tin atom concentrations were made as increasingly greater quantities of $Sn(CH_3)_4$ were added to the flame. It was also possible to obtain the $SnO(X^1\Sigma)$ concentrations in the flames from spatial absorption measurements on the SnO(A→X) (1,0), and (2,0) bands. In reducing these data, curves of growth generated for SnO in a previous flame study (ref. 1) were employed to obtain total $SnO(X^1\Sigma)$ concentrations. The results of these experiments are given in table 5 and figure 10.

The data in the table show that for the six determinations the overall quenching parameter, $k_Q^i[M_i]/A$, is approximately constant, does not increase with increasing $Sn(CH_3)_4$ as would be expected if substantial quenching by tin species were taking place, and that its average value is that appropriate to $k_Q[H_2]/A$ for this flame condition. Since

$$k_Q[SnO_x]/A < k_Q[H_2]/A \tag{17}$$

then for $[SnO_x]_{max} = 9 \times 10^{14}/cm^3$, $k_Q[H_2]/A \approx 18$

$$k_Q[SnO_x] < 2 \times 10^{-11} \text{ cm}^3/\text{molec sec} \tag{18}$$

As shown in figure 10, the concentrations of SnO(X) at the point of maximum SnO(a→X) emission scale approximately linearly with $[Sn(CH_3)_4]$, whereas [Sn] quite clearly does not. Indeed, for the high concentrations of additive, [Sn] appears to achieve a maximum value and to decrease with further $Sn(CH_3)_4$ addition suggesting that at high SnO_x concentrations, Sn may be reacting with another tin species (SnO?) to form SnO(X).

Finally, with regard to the scaling of the SnO(A→X) transitions in the flame, the data shown in table 5 indicate that [SnO(A)] does not vary linearly with the product $[Sn][N_2O]$ but is instead proportional to [SnO(X)]. This result suggests that $SnO(A^1\Pi)$ is excited primarily by processes involving $SnO(X^1\Sigma)$, for example three-body recombination reactions and, therefore, may not result directly from the Sn/N_2O reaction.

Table 5.

TIN SPECIES MEASUREMENTS AS A FUNCTION OF ADDED $Sn(CH_3)_4$

Run No.	I(a→X) Ph/cc/sec	I(A→X) Relative	$[Sn(CH_3)_4]$ Molec/cc	[Sn] /cc	[SnO] Molec/cc	$\sum_i k_Q^i [M_y]/A$
1	$0.79X10^{14}$	20	$1X10^{14}$	$0.6X10^{12}$	$0.5X10^{14}$	14.2
2	$1.9X10^{14}$	41.5	$2.6X10^{14}$	$1.5X10^{12}$	$0.70X10^{14}$	14.7
3	$2.3X10^{14}$	110	$3.5X10^{14}$	$1.8X10^{12}$	$1.7X10^{14}$	14.7
4	$3.1X10^{14}$	125	$5.6X10^{14}$	$2.3X10^{12}$	$2.0X10^{14}$	13.9
5	$2.9X10^{14}$	161	$7.0X10^{14}$	$2.4X10^{12}$	$3.1X10^{14}$	15.6
6	$2.2X10^{14}$	180	$9.0X10^{14}$	$2.0X10^{12}$	$3.7X10^{14}$	18.2

Flame: $H_2/N_2O/He$ = 1.3/1/1/3; T_{pk} = 660°K

$[N_2O] = 3.6 \times 10^{16}$ molec/cc; $[H_2] = 4.7 \times 10^{16}$ molec/cc

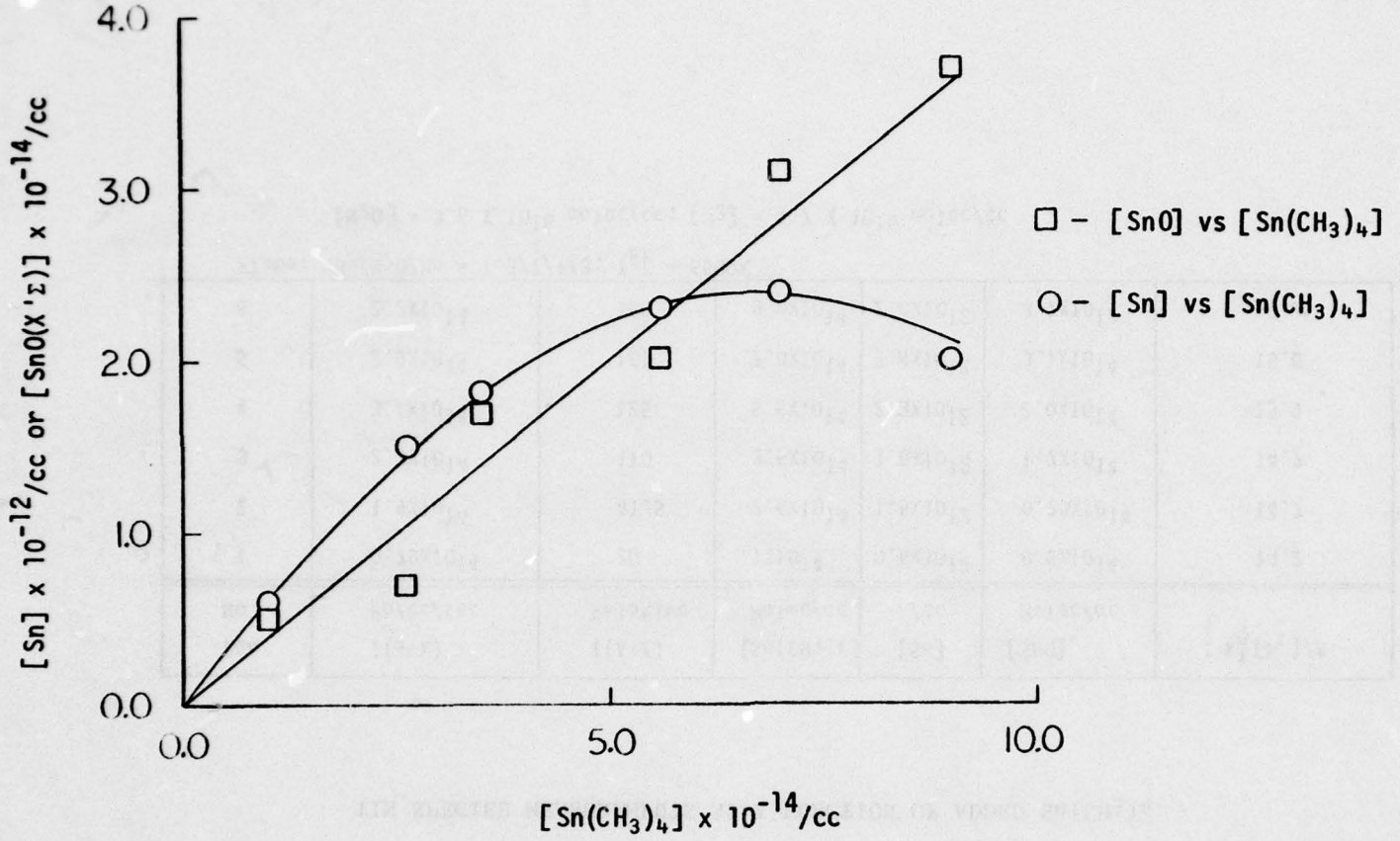

Figure 10. Sn and SnO ($X^1\Sigma$) Concentrations as a Function of Tin Tetramethyl.

In agreement with work reported previously (ref. 1), spatially resolved absorption measurements on the SnO(A→X) system showed that [SnO($X^1\Sigma$)] peaked in the region of the flame where $I_{a\rightarrow X}$ maximized and then decreased with distance in the downstream flame gases. This behavior suggests that SnO is not a final product of combustion and that reactions such as

$$SnO(X) + N_2O \rightarrow SnO_2 + N_2 \qquad (19)$$

may convert SnO to higher oxides of tin.

The quenching of SnO($a^3\Sigma$) by SnO_x was postulated by Felder and Fontijn (ref. 2) to explain the apparent fall-off of the SnO(a→X) photon yield at high concentrations of SnO_x. However, in their experiments the concentrations of atomic Sn throughout the course of the reaction were not measured. Consequently, it is possible that the decreased photon yields observed were not the result of quenching but instead reflected the loss of Sn atoms by reaction with higher tin oxides. For example, at high SnO_x concentrations it is possible that nonradiative processes such as

$$Sn + SnO_2 \rightarrow 2SnO(X) \qquad (20)$$

could effectively compete with N_2O for Sn atoms to reduce the apparent photon yields.

Based on the value of the rate constant for SnO($a^3\Sigma$) quenching by SnO suggested by Felder and Fontijn; i.e., $k_Q \approx 5 \times 10^{-10}$ cm^3/molec sec, the observed value for the quenching parameters in the high SnO_x flame experiments would be expected to be approximately an order of magnitude larger than those which were measured. Therefore, it would appear that self-quenching may not be as severe as might be predicted.

Although the explanation given for the observed scaling of [Sn] with tin additive seems attractive, alternative explanations can also be suggested. It is possible, for example, that the maximum tin atom concentration in the flames is determined by kinetics of particulate tin (liquid/solid) formation, or by the number of free radicals available for the reduction of additive to Sn. Nevertheless, the conclusions regarding the importance of self-quenching would appear to be firmly based.

f. Ancillary $Sn/H_2/N_2O$ Flame Experiments

In addition to the work on self-quenching, a number of experiments were carried out to determine whether H_2O or O_2 present in the flames can significantly quench $SnO(a^3\Sigma)$. In both sets of experiments the peak $SnO(a\rightarrow X)$ emission intensity and the corresponding Sn concentrations were measured as a function of added H_2O or O_2. The $Sn(CH_3)_4$ was used as additive since it does not react with water vapor, and the experimental data were examined to determine whether the photon yields for the $SnO(a\rightarrow X)$ transitions were appreciably affected by the potential quenchants.

Although the addition of oxygen significantly lowered the peak $SnO(a\rightarrow X)$ intensity, it was found that the decrease could be entirely attributed to the decrease in [Sn] brought about by the reaction of Sn with O_2 and that the SnO* photon yields in the flame were unaffected by O_2 quenching. From measurements of the decrease in Sn atom concentrations produced by the additions of O_2 it was possible to estimate the rate constant for the Sn/O_2 reaction; the result, $k \approx 2 \times 10^{-11}$ cm^3/molec sec, is in good agreement with that reported by Felder and Fontijn (ref. 2).

To test the quenching effect of H_2O, known partial pressures of water were added to $H_2/N_2O/He$ mixtures prior to their combustion. Known flows of vapor were produced by permitting metered amounts of liquid to be evaporated in a heated vaporizer (ref. 14) which was operated at low pressures and purged by the $H_2/N_2O/He$ flow. The peak intensity of the $SnO(a\rightarrow X)$ transitions and the corresponding tin concentrations were measured as increasing quantities of H_2O were added to a $H_2/N_2O/He$ = 1/.75/2.02 flame burned at 10 torr. It was found that neither [Sn] nor $I_{SnO(a\rightarrow X)}$ were appreciably affected by H_2O. For a flame having an unburned gas composition $H_2/N_2O/He/H_2O \approx 1/.75/2.02/.42$ the photon yield was only about 10% less than that measured in the absence of added water vapor.

On the basis of these experiments it was concluded that while a small concentration of O_2 present in the gases as a result of combustion or as an impurity can reduce the concentration of tin atoms produced in the flame, it does not significantly quench $SnO(a^3\Sigma)$. Surprisingly, water does not appear to affect either SnO* or Sn.

Several attempts to measure gain or loss on the $SnO(a\rightarrow X)$ transitions were carried out using an intracavity dye laser technique described in reference 15. In these experiments the flame was placed in tandem with a flash lamp pumped Rhodamine 6G dye cell, and both flame and cell were placed within a cavity formed by a totally

reflecting and a partially transmitting mirror. The output of the laser was examined using a spectrograph. Although the conditions and tin/tin oxide content of the 6 inch diameter flames were varied over as broad a range as possible, neither loss nor gain was observed for the (0,3), (0,4) and (0,5) SnO(a→X) transitions which lie within the spectral region of the laser dye. Since the sensitivity of this technique to gain or to absorption is quite high, ca 10^{-4}/cm, these results indicate that the high column densities of SnO($a^3\Sigma$) required to achieve laser threshold cannot be produced in the flames.

7. THE Ge/H_2/N_2O AND Si/H_2/N_2O FLAME SYSTEMS

a. Spectroscopy

The introduction of either $GeCl_4$ or GeH_4 into H_2/N_2O flames burned at pressures of from 3 to 20 torr resulted in relatively strong GeO* chemiluminescence in the preheat zone, entirely analogous to that observed when tin additives were present in the same flame. For both additives the chemiluminescence was confined to the preheat zone only -- no discrete banded emission attributable to metal oxide could be observed in the reaction zone. The spectra observed for GeH_4 and $GeCl_4$ additives are shown in figures 11 and 12, respectively.

The GeO spectrum shown in figure 11 is qualitatively similar to that observed by Capelle and Brom (ref. 4) in the reaction of Ge vapor with N_2O. Clearly observed are v' = 0,1 and 2 progressions for the $a(^3\Sigma) \rightarrow X(^1\Sigma)$ transitions as well as bands from both $A(^1\Pi) \rightarrow X(^1\Sigma)$ and $b(^3\Pi) \rightarrow X(^1\Sigma)$ transitions. Note that the spectra shown (recorded using a Spex Monochromator/EMI 6256 photomultiplier tube) are uncorrected for system response and that the apparently weak intensities associated with the A→X transitions are, in fact, stronger than the a→X transitions. It is interesting to point out in this regard that the band systems observed in the flame and in the experiments reported by Capelle and Brom (ref. 4) differ from those observed by Hager, et al (refs. 3, 16). In the latter study, it was found that the low (room) temperature reaction between Ge (formed in very low concentrations by discharge through germane) and N_2O leads exclusively to (a→X) emission. Taken collectively, these results suggest that the electronic-state distributions resulting from the Ge + N_2O interactions may be functions of the total number density at germanium species and/or the kinetic temperature.

An estimate of the vibrational temperature of GeO(a→X) was made using the relative intensity distributions from figure 11 and the relative Einstein coefficients given by Hager, et al (refs. 3 and 16). The resulting temperature was found

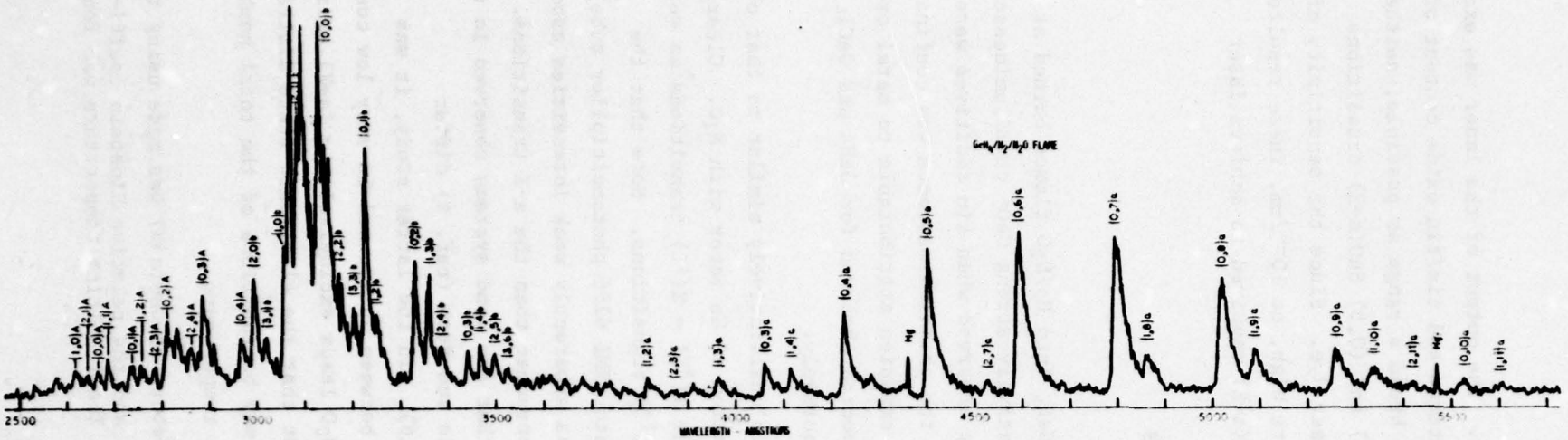

Figure 11. $GeH_4/H_2/N_2O$ Chemiluminescence Flame Spectra (Uncorrected for Detector Response)

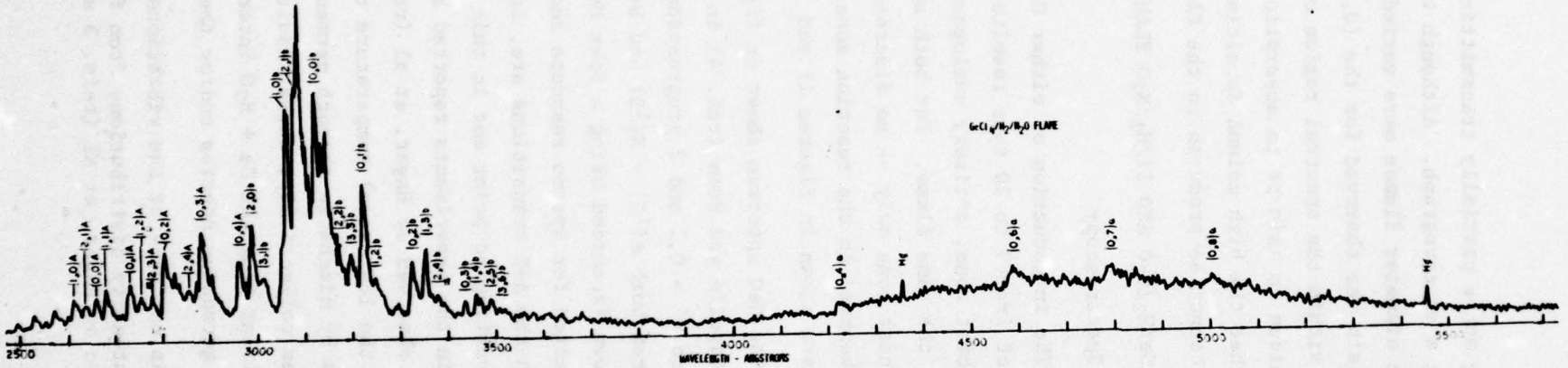

Figure 12. $GeCl_4/H_2/N_2O$ Chemiluminescence Flame Spectra (Uncorrected for Detector Response)

to be ca 530°K. Attempts were also made to reduce the data using the Franck-Condon factors tabulated by Capelle and Brom (ref. 4). This procedure led to inconsistent results suggesting possible errors in these Franck-Condon factors.

The spectrum of GeO obtained using $GeCl_4$ as additive is shown in figure 12. Most obvious in this spectrum is the weakness of the intensities of the GeO (a→X) transitions relative to those for (b→X) and A→X). Indeed the spectrum in the visible and uv appears to be dominated by a continuum-like emission, a portion of which may be from the $GeCl_2^*$. A possible explanation for the relative weakness of the (a→X) transition may be the selective quenching of $GeO(a^3\Sigma)$ by $GeCl_4$ or by $GeCl_x$, since the long radiative-lifetime of the $a^3\Sigma$ state may render it particularly susceptible to quenching.

The addition of $SiCl_4$ to the H_2/N_2O flames resulted in relatively strong continuous particulate emission in the reaction zone and no banded emission could be observed in the preheat zone. This observation indicated that $SiCl_4$ was not reduced to free Si atoms in the flame gases. In similar experiments in which SiH_4 was added to the flames, only the SiO(A→X) transitions were observed in the preheat zone. Since the SiO(a→X) transitions could not be observed, no further work was done with this system. The low vapor pressure of Si, together with the long radiative lifetime of the $SiO(a^3\Sigma)$ state would appear to preclude interest in SiO as an active laser species.

b. Interpretation of the GeO* Flame Profiles

Profile data for GeH_4 containing $H_2/N_2O/He$ = 1.3/1.0/1.3 flame burned at 9.8 torr are summarized in table 6. As observed in the $H_2/N_2O/He/Sn$ flames, the electronic Ge temperatures are substantially higher than the kinetic flame temperature, indicating Ge chemiexcitation. In general, the nearly identical behavior of both GeO* and SnO* in this flame suggests that the kinetics of the two systems are similar and that the profile analysis carried out for $SnO(a^3\Sigma)$ should apply equally well for GeO.

Recently, Felder and Fontijn (ref. 17) measured the rate constants for the reactions

$$Ge(^3P_J) + N_2O \xrightarrow{k_J} GeO + N_2O \qquad (21)$$

Table 6.

PROFILE DATA ON $H_2/N_2O/He$ FLAME WITH GeH_4 ADDITIVE

P = 9.8 torr $H_2/N_2O/He$ = 1.3/1.0/1.3

z (mm)	$I_{a\to X}$ $\times 10^{-13}$ ph/cc/sec	$[Ge^3P_0]$ $\times 10^{-11}$/cc	$[Ge^3P_1]$ $\times 10^{-11}$/cc	$[Ge^3P_2]$ $\times 10^{-11}$/cc	$[N_2O]$ $\times 10^{-16}$/cc	Temperature Kinetic °K	Temperature Electronic °K	$\sum_{J=0}^{3} k_J[Ge^3P_J]$	ϕ $\times 10^4$	$k_Q[M]/A$	$k_{Q,\ H_2}$ $\times 10^{13}$ cc/Molec/sec
1	1.60	0.57	0.70	0.30	6.01	900	900	1.1	2.4	62	1.3
2	2.55	0.61	0.80	0.39	5.59	430	980	1.3	3.5	56	1.3
3	1.77	0.62	0.85	0.44	4.76	510	1030	1.5	2.5	102	2.8
4	0.81	0.34	0.47	0.25	3.64	660	1040	0.92	2.4	97	3.5
5	0.33	0.13	0.18	0.10	2.83	850	1060	0.38	3.1	74	3.4

$k_{Q,\ H_2} = 1.1 \times 10^{-12} \exp(-837/T)$

for the $^3P_0$, $^3P_1$ and $^3P_2$ states of Ge, and found $k_{J=0}$, $k_{J=1}$, and $k_{J=2}$ to be, respectively, $(1.6\pm.3) \times 10^{-11} \exp[(-470\pm105)/T]$, $(1\pm.2) \times 10^{-11} \exp[(-62\pm105)/T]$, and $(1.2\pm.2) \times 10^{-11} \exp[(-190\pm105)/T]$. In reducing the data in table 6, it was assumed that the photon yield at each point along the flame is given by

$$\phi = I/\sum_{J=0}^{2} k_J\left[Ge\left(^3P_J\right)\right]\left[N_2O\right] \qquad (22)$$

The resulting values of ϕ are shown in table 6 along with the corresponding value of the quenching parameter, $k_Q[M]/A$, calculated using equation (10) with $\phi_o = 0.02$ (ref. 17). In contrast with the results obtained for $SnO(a^3\Sigma)$, the quenching parameter for $GeO(a^3\Sigma)$ does not appear to vary greatly over the profile, and this result suggests that the quenching of $GeO(a^3\Sigma)$ is not very temperature sensitive. If it is assumed that H_2 is the principal quenchant of $GeO(a^3\Sigma)$ and that A for this species is ca 170 sec^{-1} (ref. 13), the values for k_Q listed in the last column of table 6 are obtained. If the small increase in the quenching rate constant with distance in the flame is attributed to the increased temperature along the profile, then from a plot of k_Q vs. 1/T,

$$k_{Q,H_2} \approx 1.1 \times 10^{-12} \exp(-887/T) \text{ cc/molec sec} \qquad (23)$$

It is interesting to note that estimates were also made of the GeO* system photon yield in the flame. It was found that ϕ (system, all states) was approximately 0.0013, and that ϕ (system, a→X) was about 0.0003. The close agreement between ϕ (system) and ϕ (profile, table 6) for the GeO(a→X) transitions implies that virtually all of the GeH_4 added to the flames is converted to GeO via the Ge/N_2O reaction.

In summary, the relatively low photon yields measured in the flames result from both the inherently low branching ratio associated with the Ge/N_2O reaction and the rather substantial quenching of $GeO(a^3\Sigma)$ by a flame species, very likely H_2. The results also indicate that the possibility of achieving a population inversion in the flames is unlikely.

8. INFRARED MEASUREMENTS

A cursory infrared spectroscopic examination of SiH_4 and $SnCl_4$ containing H_2/N_2O flames was carried out to determine whether the vibrational-rotational

spectra of metal oxide species could be detected using available IR instrumentation. A Digilab Model FTS-14 interferometer equipped with a liquid nitrogen cooled Hg/Cd/Te detector was used to measure emission originating in the chemiluminescent region of the flames. Spatial resolution within the flame volume was obtained by placing two small circular apertures between the flame and the entrance optics of the interferometer. Flame (plus thermal background) spectra were measured with and without metal additives.

In flames containing relatively large initial silane concentrations; i.e., $[SiH_4] > 10^{15}/cm^3$, a small but definite emission band in the spectral region between ca 1050 and 1250 cm^{-1} has been observed. Although this emission lies in the SiO fundamental region, it could not be unequivocally attributed to this species because of the possible presence of other silicon-oxygen compounds (SiO_2?) which may also be in the flame and which would be expected to emit in the same spectral region. If the observed band did indeed arise from SiO, however, the result obtained can be of considerable interest because the shape of the band and its long wavelength limit indicated substantial populations of SiO in vibrational levels as high as $v = 16$ or greater.

In contrast to the result obtained with SiH_4, emission from SnO could not be discriminated from flame-plus-background signal levels. Because of the nature of the data which was obtained in these experiments, quantitative interpretation of the spectra were not possible and this work was not pursued further.

SECTION III

FLOW REACTOR STUDIES OF Sn/N_2O SYSTEMS

As a result of the flame measurements it was recognized that the flame environment, with its rather inflexible operating conditions, is not suitable for reaching lasing threshold. On the other hand, no information was obtained which ruled out the possibility of achieving laser action in the Sn/N_2O system given the proper conditions. To further explore this possibility and to obtain detailed kinetic information on the mechanisms for $SnO^*(a^3\Sigma)$ production and quenching it was decided to study the direct reaction of atomic tin and N_2O. Hopefully, these measurements would further substantiate the quenching results obtained in the flame and perhaps suggest a better approach to the problem of attaining lasing threshold.

Felder and Fontijn (ref. 2) have reported kinetic measurements for this system using their high temperature, fast flow reactor. However, they do not report quenching information for hydrogen and only give overall global kinetics for the $Sn + N_2O$ reaction without detailing rates of reaction for the individual tin (i.e., $^3P_0$, $^3P_1$, $^3P_2$) ground state species.

In the experiments reported here, the individual rates of reaction of $Sn\,^3P_0$ and $Sn\,^3P_1$ with N_2O and the quenching of $^3P_1$ and SnO^* were investigated. Furthermore, these reactions were studied in a manner which eventually would be more suitable for lasing since long optical path lengths and fast flows were used.

1. EXPERIMENTAL

Since this effort represented only a small percentage of the overall program, attempts were made to utilize existing equipment with a minimum of modification. To this end, our fast flow, rectangular cross section, flow reactor was used in conjunction with a metal vapor generator identical in design to that employed in the electrical copper vapor laser development program (refs. 18, 19). Since the flow reactor was of modular construction, the metal vapor generator was easily installed into the upstream section of the flow reactor where it replaced the microwave discharge atom source of the original apparatus.

Briefly, the metal vapor generator source consists of a hollow graphite injector strip approximately 10 x .5 x 2 cm. One lid of the injector contains a hole array composed of .038 cm diameter holes drilled on 0.050 cm centers. The surface

of the array is approximately 51 percent open area. The opened ends of the injector strip are inserted into appropriate slots contained in two cylindrical graphite reservoirs. These reservoirs were made in the shape of a hollow tube with one end closed and injector slots placed just above the closed end. The device is heated electrically, and in the experiments to be described approximately 3 to 4 kw were used to vaporize the quantities of tin needed.

To avoid major equipment modifications, the generator was mounted in a position so that: (a) tin atoms were vaporized perpendicular to the main carrier flow and (b) located approximately 12 cm upstream from the location at which N_2O was injected into the tin atom-carrier gas mixture. Unfortunately, this nonoptimal geometry severely limited the flux of tin atoms available for reaction. Any future apparatus would have the metal generator and N_2O injectors as close together as possible. A schematic of the apparatus in shown in figure 13. The reactor section of the device is made of stainless steel and contains a rake array which makes possible rapid mixing of reactants. Each tube of the rake array is made of stainless steel, and contains seven holes approximately 0.025 cm in diameter through which N_2O or other gases are injected perpendicular to the main flow. There are a total of 20 injector tubes, each approximately 1.3 cm long and spaced equally along the 15 cm width of the reactor section, Optical measurements could be made through Brewster-angled windows in the volume of gas extending from the injector tubes to a point approximately 10 cm downstream. The reaction section of the device was heated by resistive elements placed in contact with the walls. Maximum wall temperatures of approximately 600 $^{\circ}K$ could be maintained without noticeable deterioration of O rings and gasket materials used in assembling the flow reactor.

Carrier gases entered the rear of the reactor, entrained tin atoms from the generator strip and the mixture, upon entering the reactor section, was mixed with N_2O or other species. Emission and absorption measurements were carried out on the flowing reactive mixture after which the gas exited through an expansion section into a dump tank and was exhausted by a 1200 cfm Roots blower. Total flows were such as to result in flow velocities as high as 1.5×10^4 cm/sec. Pressures in the reactor section could be maintained as low as two torr under maximum flow conditions.

Flow within the reactor was assumed to be subsonic, compressible and viscous. However, examination of the compressible, constant pressure solutions for the case

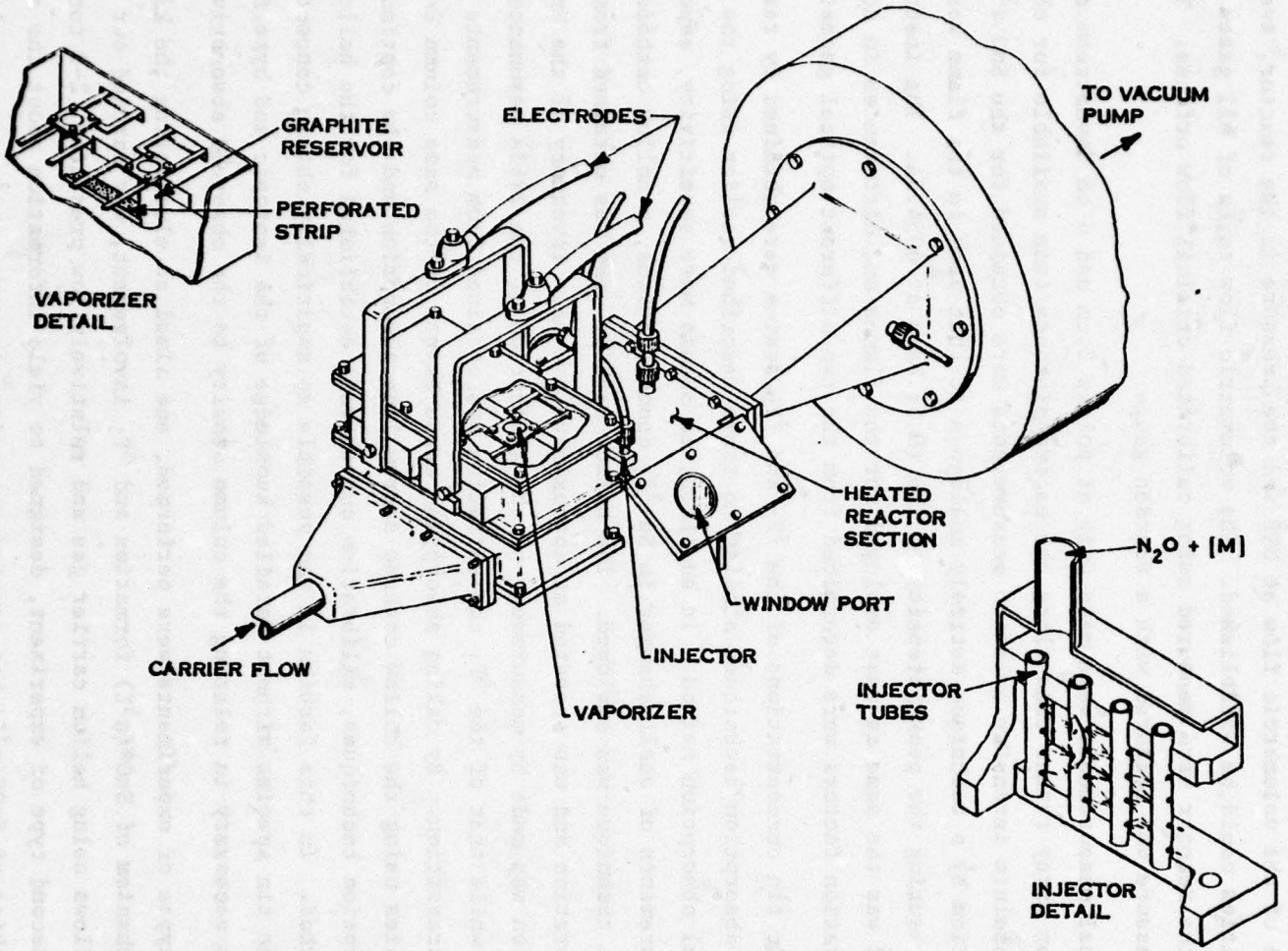

Figure 13. Flow Reactor with Tin Atom Generator

under consideration (ref. 20) showed the density/temperature variations to be negligible. Consequently, incompressible velocity profiles could be assumed and from a knowledge of the volumetric flow at NTP and the pressure in the reactor, average flow velocities could be established. The volumetric flow rates of all gases admitted to the reactor were measured using calibrated critical flow orfices. The reactor pressure was measured with a Bourdon gauge.

Optical measurements were made only at points 2 cm and 4 cm downstream of the injector array rather than along the entire distance/time available for observation. Absolute intensity emission measurements were obtained for the SnO $a^3\Sigma \rightarrow X^1\Sigma$ transition by a technique entirely analogous to that used in the flame work, viz., by measuring the peak intensity of the (0,5) band at 6064.5A. The instrumentation used was the same as that employed for the flames and differences in absolute calibration factors were determined from the two different optical geometries.

Atomic tin concentrations of the $^3P_0$ and $^3P_1$ states were obtained by resonance line absorption techniques similar to those described earlier using the continuum total absorption method. In addition, to obtain more sensitivity, especially in measurements of small changes in Sn $^3P_1$ concentrations, a hollow cathode, narrow line technique was employed. The hollow cathode used was obtained from the Oriel Corporation and was operated at approximately 6 mA. Inventory of the Sn $^3P_0$ concentration was made by measurement of the absorption of the 2863Å resonance transition while that of the $^3P_1$ concentration was obtained from measurements on the 3009Å transition. By making absorption measurements on the same column density of tin species using the hollow cathode narrow line absorption and the continuum total absorption techniques, calibration curves were established for the hollow cathode method. In this fashion it was possible to empirically obtain concentrations of the tin species without detailed knowledge of the isotopic and hyperfine corrections necessary in relating the column density to the observed absorbtivity.

Two types of experiments were performed, one aimed at elucidating the kinetics and mechanism of SnO*($a^3\Sigma$) formation and $^3P_1$ involvement, was carried out with very fast flows using helium carrier gas and relatively low pressures (2-3 torr) while the second type of experiment, designed to yield information about the subsequent quenching of SnO*($a^3\Sigma$) was carried out using nitrogen carrier gas at slower flows and higher pressures ($\sim$ 10 torr). In both experiments the tin generator strip was heated to approximately 1600 °K and the carrier gas flow adjusted to give

maximum tin species absorption. Attempts to increase the tin concentration by increasing the generator temperature resulted in a decrease in tin indicating a complex flow-nucleation relationship. Hopefully, this kind of behavior can be greatly reduced by reorientation by the generator strip as suggested earlier. Quenchant gases were premixed with the N_2O in known proportions and the mixture allowed to react with the flow of tin species via the injector tubes.

2. RESULTS AND CONCLUSIONS

a. Spectroscopic and General Observations

The addition of N_2O to the Sn/He or N_2 flow in the mixing section of the reactor was observed to result in fairly intense emission which persisted throughout the entire reactor section. In contrast to the flame results and to observations by other investigators (ref. 2), the emission was yellow-green in color rather than the usual blue-white. Correspondingly, spectroscopic measurements of the chemiluminescence indicate that the emission appears to be due to the SnO($a^3\Sigma \rightarrow X^1\Sigma$) transitions. No evidence, at a flow reactor temperature of approximately 500 K, for the $A^1\Sigma \rightarrow X^1\Sigma$, $b' \rightarrow X^1\Sigma$ and $b^3\pi \rightarrow X^1\Sigma$ transition was obtained. The resulting a→X spectrum, which is now free of any interferences from overlapping b→X transitions, fully confirms the assignment previously given for the a→X system. It is interesting to note that the reaction of Sn with N_2O under the flow reactor conditions appears to lead exclusively to the formation of SnO in the $a^3\Sigma^+$ state. The formation of the other SnO electronic states, as observed in the flames and in hotter flow reactor experiments, must result from subsequent reactions involving $a^3\Sigma$ or $X^1\Sigma$ SnO or be due to the reactions of tin with the possible decomposition products of N_2O.

In the experiments carried out at low pressures with fast flows of helium as the main carrier gas, it was found that appreciably larger concentrations of $^3P_1$ tin were present than that predicted for thermal equilibrium. Apparently, helium is a poor relaxer of the $^3P_1$ state and, consequently, since the tin was generated at high temperatures ($\sim$ 1600 °K), the $^3P_1$ population at the point of observation under fast flow conditions was only partially relaxed. On the other hand, in those experiments performed at higher pressures using N_2 as the carrier gas, the $^3P_1$ concentrations were much smaller indicating substantial relaxation. This fact is especially noted since it was discovered that the intensity of the SnO a→X transition appeared to vary primarily with the $^3P_1$ population. This was established by

changing the concentrations of $^3P_1$ by reaction with N_2O, by quenching with hydrogen or by varying the tin generator strip temperature. To remove any ambiquity because of the simultaneous quenching of $SnO^*(a^3\Sigma)$ by hydrogen, several experiments were carried out where the same quantity of hydrogen was added either to the rear carrier gas flow or to the N_2O injector gas flow. In this way the quenching effect on $^3P_1$ or $SnO^*(a^3\Sigma)$ could be differentiated.

It is believed that Sn^3P_0 also contributes directly, albeit with a much smaller rate constant, to the formation of $SnO^*(a^3\Sigma)$. Nevertheless, it is felt that the primary mechanism of SnO* formation involves the reaction of $^3P_1$ with N_2O. Analysis of a limited number of observations appears to be consistent with this premise. Tentative rate constants for the reactions of Sn^3P_1 with N_2O and the corresponding branching ratio for the light producing reaction have been obtained. Quenching constants of $^3P_1$ by hydrogen and nitrogen have also been measured.

From the higher pressure, slower flow studies, it was possible to measure the quenching of $SnO^*(a^3\Sigma)$ by various species. This was done in detail for hydrogen because of its relevance to the flame work.

b. Overall Sn^3P_1 Removal Kinetics

Under conditions of fast flows (short times) and low pressures, where the $Sn^3P_1 + N_2O$ reaction appears to dominate the formation of SnO*, the following kinetic treatment was used to analyze a limited number of observations at approximately 550 °K and 300 °K.

Consider the following sequence of reactions

$$Sn^1 + M \underset{k_Q^{-1}}{\overset{k_Q^1}{\rightleftharpoons}} Sn^0 + M \qquad (24)$$

$$Sn^1 + N_2O \xrightarrow{k_T^1} SnO\ (total) + N_2 \qquad (25)$$

$$Sn^1 + N_2O \xrightarrow{k^{1*}} SnO(a^3\Sigma) + N_2 \qquad (26)$$

$$SnO^* \xrightarrow{A} SnO + h\nu \qquad (27)$$

$$SnO^* + M \xrightarrow{k_Q} SnO + M \qquad (28)$$

where

$$Sn^1 = Sn^3P_1,\ Sn^0 = Sn^3P_0$$

Reaction (25) represents the total production of SnO in all states including the $X^1\Sigma$ ground state, while (26) and (27) represent the light producing reactions and (28) the collisional quenching of SnO*. As will be seen, under the fast flow conditions, reactions (24), (25) and (26) dominate the kinetics since (27) and (28) are much slower processes. Nevertheless, these latter reactions have been included in the analysis. Since $[M] >> [Sn^1]$ or $[Sn^0]$, where M includes N_2O, the products of $[M]$ or $[N_2O]$ with the various rate constants can be considered to remain constant making possible the use of pseudo first-order kinetic treatment.

Let

$$k_Q[M] = \beta^1,\ k^{-1}[M] = \beta^{-1},\ k_T[N_2O] = \alpha^1$$

$$k^{1*}[N_2O] = \alpha^{1*},\ \text{and}\ A + k_Q[M] = \beta$$

Then

$$\frac{d[Sn^1]}{dt} = -(\alpha^1 + \beta^1)\,[Sn^1] + \beta^{-1}\,[Sn^0] \qquad (29)$$

Since the change in $[Sn^0]$ due to reaction (24) is very small (at early times) compared to the total $[Sn^0]$ present, $[Sn^0]$ can be taken as constant in equation (29). Therefore, upon integration of (29)

$$[Sn^1] = \left([Sn^1_0] - \left[Sn^1_{s.s.}\right]\right) \exp-(\alpha^1 + \beta^1)t + \left[Sn^1_{s.s.}\right] \qquad (30)$$

where

$[Sn^1_0]$ is the initial $^3P_1$ concentration and

$\left[Sn^1_{s.s.}\right] = \beta^{-1}[Sn^0]/(\alpha^1 + \beta^1)$ can be considered to be the steady-state concentration of Sn^1. By rearranging (30) so that

$$\frac{[Sn^1] - \left[Sn^1_{s.s.}\right]}{[Sn^1_0] - \left[Sn^1_{s.s.}\right]} = \exp-(\alpha^1 + \beta^1)t \qquad (31)$$

and considering the case where $[M] = [N_2O]$, a plot of the $\ln\left(\left[Sn^1\right] - \left[Sn^1_{s.s.}\right]\right)/\left(\left[Sn^1_0\right] - \left[Sn^1_{s.s.}\right]\right)$ vs. $[N_2O]t$ should yield a straight line whose slope is equal to $-(k^1_T + k^1_Q)$. This procedure was used in the analysis of several experiments carried out at 550 and 300 °K. Data for two typical sets of measurements and the resulting plots of equation (31) are given in figure 14. The complete set of results are given in table 7. The value of 9×10^{-13} (ref. 2) for the overall removal rate constant at 315 °K is in good agreement with values reported in table 7.

Quenching rate constants of Sn^3P_1 by hydrogen and nitrogen were obtained in a manner completely analogous to the above method. These measurements were carried out at approximately 550 °K using helium as the bath (carrier) gas by observing the changes in $^3P_1$ concentrations when either H_2 or N_2 was added to the flow through the injector array. These results are given in table 8. A comparison with the recent room temperature results reported by Foo, et al (ref. 21) suggests that there is a small activation energy to be associated with the respective quenching, since the rate constant values at 550 °K appear to be somewhat larger.

For the N_2O studies, it was possible to estimate the contribution to the overall removal rate constant by the individual rate constants k^1_T and k^1_Q. This was done for Run #1 of table 7 at 550 °K in the following manner:

For a given addition of N_2O the changes in $[Sn^3P_1]$ and $[Sn^3P_0]$ were obtained from the respective absorption measurements. The corresponding rate equations for reactions (24) and (25) yield

$$d[Sn^0]/dt = \beta^1[Sn^1] - \beta^{-1}[Sn^0] \tag{32}$$

and

$$d[Sn^1]/dt = -(\alpha^1 + \beta^1)\,[Sn^1] + \beta^{-1}[Sn^0] \tag{33}$$

so that

$$\Delta Sn^0/\Delta Sn^1 \approx \frac{\beta^1/(\alpha^1 + \beta^1)\,[Sn^1]/\left[Sn^1_0\right] - \left[Sn^1_{s.s.}\right]/\left[Sn^1_0\right]}{-[Sn^1]/\left[Sn^1_0\right] + \left[Sn^1_{s.s.}\right]/\left[Sn^1_0\right]} \tag{34}$$

For the addition of 3.3×10^{15} molec/cc of N_2O, $\Delta Sn^0/\Delta Sn^1 = -.44$

$$\overline{[Sn^1]}/\left[Sn^1_0\right] \approx .8, \text{ and } \left[Sn^1_{s.s.}\right]/\left[Sn^1_0\right] \approx .12$$

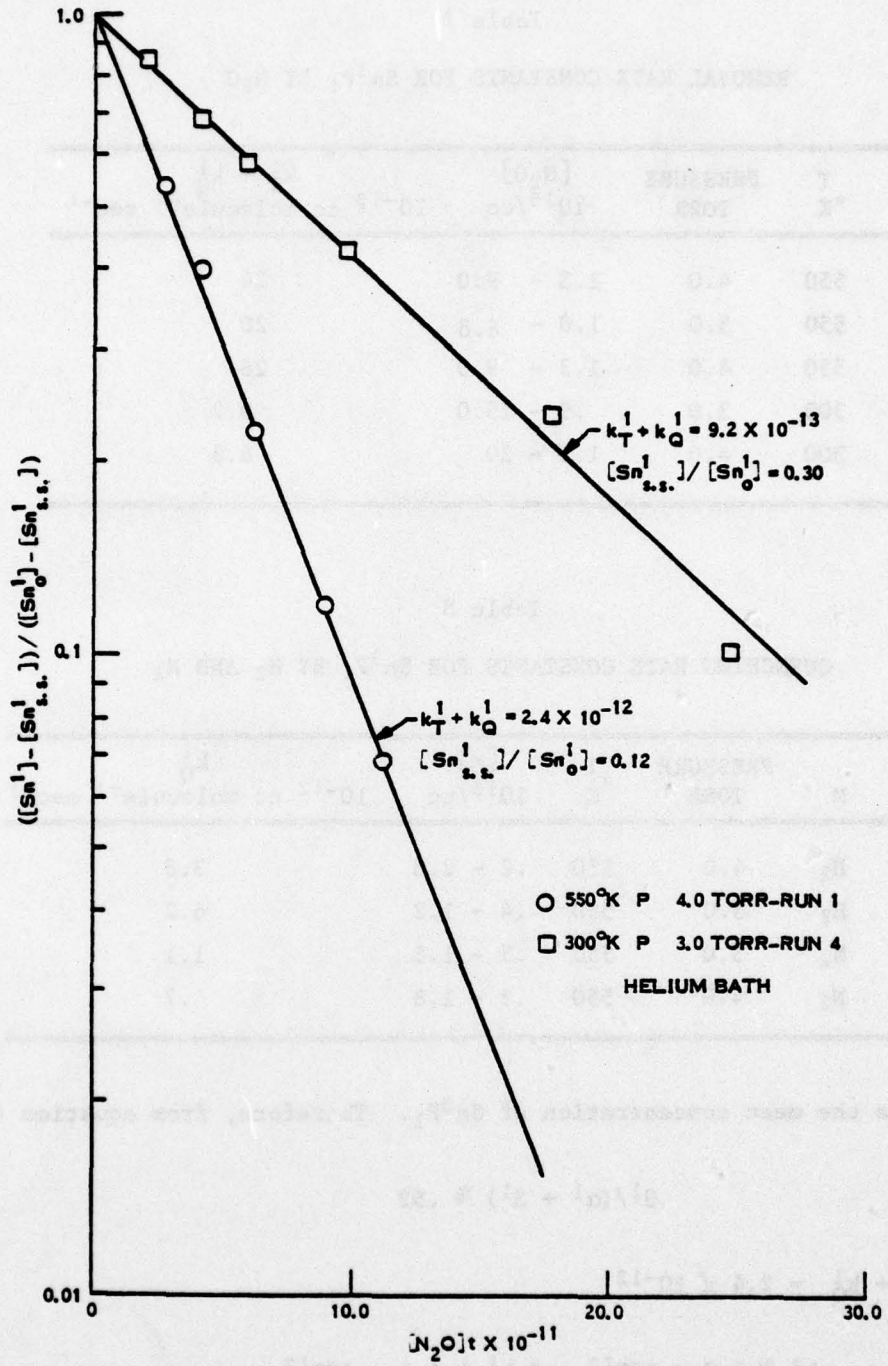

Figure 14. Typical Sn^3P_1 Removal Rate Constant Analysis Plots

Table 7

REMOVAL RATE CONSTANTS FOR Sn^3P_1 BY N_2O

RUN NO.	T °K	PRESSURE TORR	$[N_2O]$ 10^{15}/cc	$k_T^1 + k_Q^1$ 10^{-13} cc molecule^{-1} sec^{-1}
1	550	4.0	1.3 - 9.0	24
2	550	3.0	1.0 - 6.8	20
3	550	4.0	1.3 - 9.0	28
4	300	3.0	.9 - 15.0	9.2
5	300	4.0	1.2 - 20	6.8

Table 8

QUENCHING RATE CONSTANTS FOR Sn^3P_1 BY H_2 AND N_2

RUN NO.	M	PRESSURE TORR	°T K	[M] 10^{15}/cc	k_Q^1 10^{-12} cc molecule^{-1} sec^{-1}
1	H_2	4.0	550	.2 - 2.0	3.8
2	H_2	3.0	550	.4 - 1.2	6.2
3	N_2	3.0	550	.5 - 1.5	1.1
4	N_2	4.0	550	.3 - 1.8	.7

where $\overline{[Sn^1]}$ is the mean concentration of Sn^3P_1. Therefore, from equation (34),

$$\beta^1/(\alpha^1 + \beta^1) \approx .52 \qquad (35)$$

and since $k_T^1 + k_Q^1 = 2.4 \times 10^{-12}$

$$k_Q^1 \approx 1.3 \times 10^{-12} \text{ and } k_T^1 \approx 1.1 \times 10^{-12}$$

The value of $k_Q^1 = 1.3 \times 10^{-12}$ for N_2O quenching is not very different from the quenching constant for N_2, a result which is not unexpected. On the other hand the

reactive constant $k_1^1 = 1.1 \times 10^{-12}$ is approximately a factor of 25 larger than the overall tin removal rate constant (ref. 2).

c. $SnO^*(a^3\Sigma)$ Formation Kinetics

The net formation rate of SnO* is obtained from reactions (26), (27) and (28); i.e.

$$d[SnO^*]/dt = \alpha^1 * [Sn^1] - \beta[SnO^*] \tag{36}$$

setting

$$[Sn^1] = \left(\left[Sn_0^1\right] - \left[Sn^1{}_{s.s.}\right]\right) \exp-(\alpha^1 + \beta^1)t + \left[Sn^1{}_{s.s.}\right]$$

and integrating (36) yields

$$[SnO^*] = \frac{\alpha^1 * \left(\left[Sn_0^1\right] - \left[Sn^1{}_{s.s.}\right]\right)}{\alpha^1 + \beta^1 - \beta} [\exp-(\beta t) - \exp-(\alpha^1 + \beta^1)t]$$

$$+ \frac{\alpha^1 * \left[Sn^1{}_{s.s.}\right]}{\beta} [1 - \exp-(\beta t)] \tag{37}$$

Rearranging (37) and setting

$$I = \frac{\left(\left[Sn_0^1\right] - \left[Sn^1{}_{s.s.}\right]\right)}{\alpha^1 + \beta^1 - \beta} [\exp-(\beta t) - \exp-(\alpha^1 + \beta^1)t]$$

$$II = \left[Sn^1{}_{s.s.}\right] [1 - \exp-(\beta t)]/\beta$$

so that

$$[SnO^*]/\alpha^1 * = I + II \tag{38}$$

or

$$I + II = [SnO^*]/k^1 * [N_2O] \tag{39}$$

For the case where $[M] = [N_2O]$ it is seen that a plot of I + II versus $[SnO^*]/[N_2O]$ should give a straight line with a slope equal to $1/k^1*$. This procedure was followed for runs 1-5 of table 7. In evaluating the terms I and II,

$\alpha^1 + \beta^1$ were obtained using the overall removal rate constants and multiplying by $[N_2O]$; and β was calculated by assuming the radiative transition probability, A, to be equal to 1000 and $k_Q^{N_2O}$ to be equal to 10^{-14} (ref. 2). Typical plots of equation (39) for runs 1 and 4 of Table 7 are shown in figure 15. The results for all the measurements are given in table 9. A least square fit of these data gives the following expression for the light producing rate constant as a function of temperature:

$$k^{1*} = 2.8 \pm 1.1 \times 10^{-11} \exp(-1990/T) \qquad (40)$$

Table 9

LIGHT PRODUCING RATE CONSTANT, k^{1*}, FOR THE REACTION OF Sn^3P_1 WITH N_2O

RUN NO.	T °K	PRESSURE TORR	N_2O 10^{15}/cc	k^{1*} 10^{-13} cc molecule^{-1} sec^{-1}
1	550	4.0	1.3 - 9.0	8.2
2	550	3.0	1.0 - 6.8	6.0
3	550	4.0	1.3 - 9.0	9.0
4	300	3.0	.9 - 15.0	.47
5	300	4.0	1.2 - 20.0	.30

Since this expression is based only on measurements taken at two different temperatures, the error associated with the apparent activation energy ($\sim$ 4 Kcal/mol) can conceivably be quite large. Nevertheless, it is obvious that the rate constant for the reaction of Sn^3P_1 with N_2O is considerably greater, in the temperature range of interest, than that for the overall reaction of Sn (total) with N_2O as given in reference 2. An estimate of the branching ratio, k^{1*}/k_T^1, at 550 °K can be made using these results. This ratio was found to be approximately equal to .7 ± .4 indicating that the reaction of Sn^3P_1 with N_2O proceeds primarily through the light producing channel.

The relative contribution to the SnO* emission by the reaction of Sn^3P_0 with N_2O was obtained through a series of experiments in which the ratio of $^3P_1/^3P_0$ was varied by changing the temperature of the vaporizer strip. This procedure was

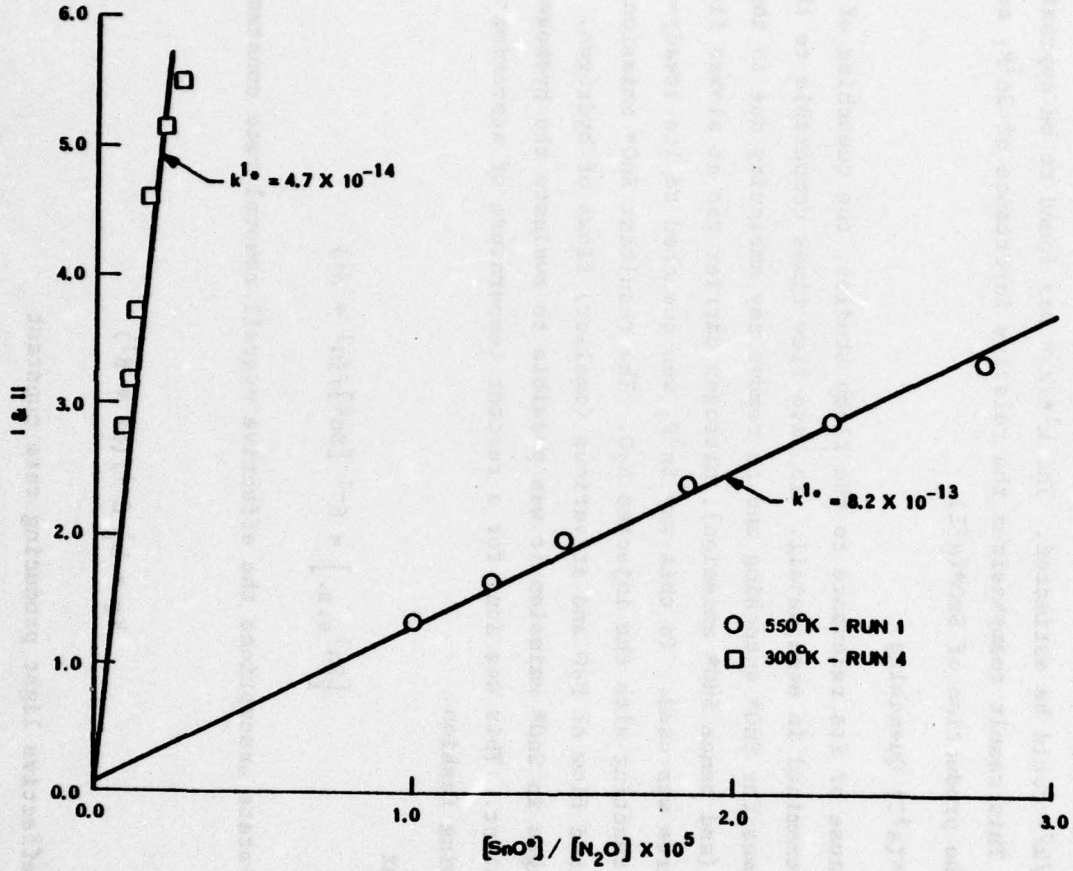

Figure 15. Typical $^3P_1$ Light Producing Rate Constant Analysis Plots

carried out at the reactor temperature of approximately 550 °K. Assuming that the total SnO* emission intensity, at early times, could be approximated by

$$SnO^* \sim c\ k^{1*}\ [Sn^1] + k^{0*}\ [Sn^0] \tag{41}$$

where $c \sim .85$, by measuring SnO* at various relative concentrations of Sn^1 and Sn^0, the ratio k^{1*}/k^{0*} could be estimated. The k^{1*}/k^{0*} was found to be approximately equal to 40. This result reemphasizes the relative importance of Sn^3P_1 as compared to Sn^3P_0 in the production of $SnO^*(a^3\Sigma)$.

d. $SnO^*(a^3\Sigma)$ Quenching

Because of its relevance to the flame studies, the quenching of SnO* by hydrogen was examined in some detail. To have flow times comparable to the expected 1/e times for SnO* quenching and to remove any ambiguity due to the quenching of Sn^3P_1 (and hence SnO* emission), nitrogen carrier gas at slower flows and higher pressures was used. In this way Sn^3P_1 was quenched to its steady-state value before reacting with the injected N_2O. The resultant SnO* emission was measured at a fixed flow of N_2O and at various (smaller) flows of hydrogen. From the relative changes in SnO* emission it was possible to evaluate the hydrogen quenching rate constant. This was done for a reactor temperature of approximately 550 °K in the following fashion.

Recalling that

$$\left[Sn^1{}_{s.s.}\right] = \beta^{-1}\ [Sn^0]/(\alpha^1 + \beta^1) \tag{42}$$

under steady-state assumptions the effective overall removal rate constant of Sn^0 becomes

$$k_T = k_T^1\ \beta^{-1}/(\alpha^1 + \beta^1) \tag{43}$$

and for the effective light producing rate constant

$$k^* = k^{1*}\ \beta^{-1}/(\alpha^1 + \beta^1) \tag{44}$$

Using the rate constants obtained earlier, it is possible to evaluate the quantity $\beta^{-1}/(\alpha^1 + \beta^1)$ by assuming microscope reversibility (i.e., $\beta^{-1}/\beta^1 = Keq$) and

$[M] = [N_2] >> [N_2O]$ or $[H_2]$. Note that the effective overall constant obtained in this fashion compares well, within the experimental error, to the overall constant predicted by the expression given by Felder and Fontijn. Therefore, $^3P_0$ concentrations as a function of time becomes

$$[Sn^0] = \left[Sn_0^0\right] \exp(-\alpha t) \tag{45}$$

where $\alpha = k_T[N_2O]$. Substituting (42), (44) and (45) into (36) gives

$$[SnO^*] = \frac{\alpha^*\left[Sn_0^0\right]}{\beta - \alpha} [\exp(-\alpha t) - \exp(-\beta t)] \tag{46}$$

where $\alpha^* = k^*[N_2O]$ and β contains the quenching terms for $[SnO^*]$ (i.e., $\beta = A + \sum_i k_Q^i[M_i]$). By measuring SnO* emission at constant $[N_2O]$, $[Sn_0^0]$ and $[N_2]$ and varying $[H_2]$ the quenching constant $k_Q^{H_2}$ is obtained. These results appear in table 10.

Quenching by several hydrocarbons were also very briefly investigated in a qualitative manner. On a comparative basis the results were that the quenching of $C_2H_2 > C_2H_4 > C_2H_6 > CH_4 > H_2$.

Table 10

QUENCHING RATE CONSTANT OF SnO* ($a^3\Sigma$) BY HYDROGEN

RUN NO.	[SnO*] REL	TEMP °K	$[N_2O]$ 10^{-16}/cc	$[H_2]$ 10^{-15}/cc	$[\beta-\alpha]^a$ sec^{-1}	$k_Q^{H_2}$ 10^{-13} cc $molecule^{-1}$ sec^{-1}
1	10.8	550	2.3	0	772	---
	6.6			2.3	1810	3.9
	3.6			6.8	3450	3.4
2	13.9	550	4.4	0	562	---
	9.1			2.2	1350	3.1
	4.7			6.6	3050	3.0

[a] $[k_T = 3.4 \times 10^{-14}, k_Q^{N_2O} = 10^{-14}, k_Q^{N_2} = .6 \times 10^{-16}]$; $t \approx 1.4 \times 10^{-3}$ sec.

SECTION IV

COMPARISON OF FLAME AND FLOW REACTOR RESULTS

As was indicated by the flame studies and confirmed by the flow reactor investigation, hydrogen quenching of SnO* appears to be moderately fast. The quenching rate constants obtained by the two techniques agree within a factor of three when compared at 550 °K. Although the activation energy for the quenching was not measured in the flow reactor, the value deduced from the flame studies of approximately 6.8 Kcal/mole is entirely reasonable if the quenching process is reactive in nature. For example, a process such as

$$SnO^* + H_2 \rightarrow SnOH + H \qquad (47)$$

according to the very approximate Hirschfelder 5% rule (ref. 21), should have an activation energy of approximately 5 Kcal/mole.

The rate constant for SnO* quenching by hydrogen in the flame experiments was obtained assuming that the $^3P_0$, $^3P_1$ and $^3P_2$ concentrations of tin contributed equally to the production of $SnO(a^3\Sigma)$. However, the flow reactor studies clearly indicate that the flame data should have been reduced using $[Sn(^3P_1)]$ and k^{1*} rather than $[Sn_t]$ and k_T, equation (9). The quenching parameters contained in table 3 have been recalculated on this basis and the hydrogen quenching rate constant deduced in this manner was found to be approximately $k_Q^{H_2} = 6.5 \times 10^{-11} \exp(-2190/T)$ cc/molec sec. Therefore, hydrogen quenching in the flame appears to be greater than given by the original calculation. At 550 °K this rate constant is approximately a factor of 4 larger than that obtained from the flow reactor study. Considering the approximate nature of the k^{1*} values used in these recalculations the agreement between the two experiments appears reasonable.

It can be concluded that quenching of SnO* by hydrogen is a severe limitation, and many methods relying on the reduction of encapsulated tin compounds for producing large amounts of tin atoms are not attractive for laser potential. Furthermore, the flow reactor study also indicates that hydrocarbon fueled/N_2O/tin additive flames provide even poorer quenching environments than that of hydrogen/N_2O for the production of SnO*.

SECTION V

CONCLUSIONS AND RECOMMENDATIONS

Although the use of premixed low pressure H_2/N_2O flames containing volatile tin and germanium compounds are convenient sources for producing electronically excited SnO and GeO, their potential for achieving threshold concentrations of these species is not good. The results of the flame study clearly demonstrate that quenching of the most likely laserable state (i.e., $a^3\Sigma$ for both SnO and GeO) by hydrogen is very severe under flame conditions. Furthermore, at typical flame residence times secondary reactions involving possible higher metal oxide species or particle formation can limit the quantities of metal atoms available for reaction with N_2O. Consequently, it is concluded that the flame approach offers little hope of producing a group of IV-A metal oxide chemically pumped electronic laser.

On the other hand, the results of the flow reactor study indicate that the direct reaction of tin atoms with N_2O produces predominantly the $SnO^*(a^3\Sigma^+)$ state and that the reaction can be rapid provided that an appreciable fraction of the tin is present in the $^3P_1$ excited state. Furthermore, under flow reactor conditions quenching of SnO* should not be limiting since the time scale for reaction can be made short compared to typical quenching times.

It is believed that the pumping reaction between $Sn\,^3P_1$ and N_2O offers a high probability for achieving gain in the $a^3\Sigma^+$ state of SnO provided sufficient concentration of the metastable tin atoms can be produced. It is suggested that by operating the metal vapor generator at approximately 2000 °C and by mixing the N_2O into the tin-carrier gas flow as close to the vaporizer source as possible that $Sn\,^3P_1$ concentrations in the range of 2×10^{16} molecules/cc can be produced. For this concentration and assuming a 10 cm path length and a reaction temperature of approximately 600 °K, the small signal gain has been estimated to be approximately 0.5%. This value was obtained using the rate constants, kinetic analysis and molecular properties that have been generated for tin oxide.

It is believed that the possibility of obtaining these conditions is within the capability of our present experimental facility.

REFERENCES

1. Linevsky, M. J., and R. A. Carabetta, Chemical Laser Systems, GE Rpt No. 75SDS4271, General Electric Company, Philadelphia, Pa., 1975.

2. Felder, W., and A. Fontijn, Kinetics and Molecular Spectroscopy of the Sn/N_2O Electronic Transition Chemical Laser Candidate Reaction, Aerochem Research Laboratory, Inc., Princeton, N.J., 1976.

3. Hagar, G. D., L. Wilson, and S. Hadley, Chem. Phys. Lett., Vol. 27, p.439 (1974).

4. Capelle, G. A., and J. M. Brom, Jr., Journal of Chem. Phys., Vol. 63, p.5168 (1975).

5. Mitchell, A. C. G., and M. W. Zemansky, Resonance Radiation and Excited Atoms, Cambridge University Press, 1961.

6. Vidale, G. L., "Measurements of the Vapor Pressure of Atomic Species from Spectrophotometric Measurements of the Absorption of Resonance Lines Vs Free Energy of Formation of TiC and ZrC," Report #R61SD147, General Electric Co., Philadelphia, Pa.

7. Honig, R. E., and D. A. Kramer, "Vapor Pressure Data for the Solid and Liquid Elements," RCA Review, Vol. 30, p.285, 1969.

8. Penkin, N. B., and I. Yu. Yu. Slavanas, "Oscillator Strengths of Spectral Lines SnI and PbI," Optics and Spectroscopy, Vol. 15, p.83 (1963).

9. Corliss, C. H., and W. R. Bozman, "Experimental Transition Probabilities for Spectral Lines of Seventy Elements," N.B.S., Monograph 53, 1962.

10. Lawrence, G. M., Aerosphysical Journal, Vol. 48, p.261. 1967.

11. Kaskan, W. E., Sixth Symposium (International) on Combustion, Reinhold Publishing Corporation, New York (1957).

12. Suchard, S. N., "Spectroscopic Constants for Selected Heteronuclear Diatomic Molecules," Vol. III, Aerospace Report No. TR-0074(4641)-6

13. Smith, J. J., and B. Myer, Journal of Mol. Spect., Vol. 27, p.204, 1968; B. Meyer, et al., Journal of Chem. Phys., Vol. 53, p.3616, 1970.

14. Linevsky, M. J., and R. A. Carabetta, Chemical Laser Systems, Semiannual Report, Rpt No. 73SD4278, General Electric Company, Philadelphia, Pa., 1973.

15. Anthony, E. N., et al., Optics Comm., Vol. 15, p.99, 1975.

16. Hagar, G., R. Harris, and S. Hadley, Journal of Chem. Phys., Vol. 63, p.2810 (1975).

17. Fontijn, A., Kinetic Spectroscopy of Metal Atom/Oxidizer Chemiluminescent Reactions for Laser Applications, AeroChem TN-175, AeroChem Research Laboratories, Inc., Princeton, N. J., 1977.

18. Linevsky, M. J., and R. A. Carabetta, Combustion Lasers, Report No. 73SD4223, General Electric Company, Philadelphia, Pa., 1973.

19. Karras, T. W., et al, Copper Vapor Generator, Final Technical Report No. AFWL-TR-73-133, June 1973.

20. Linevsky, M. J., and F. N. Alyea, Spectroscopy of Metal Oxides, Technical Report No. RADC-TR-73-391, November 1973.

21. Foo, P. D., et al, Journal of Phys. Chem., Vol. 80, p.91, 1976.

22. Hirchfelder, J. D., Journal of Chem. Phys., Vol. 9, p.645, 1941.